NJC

PERSPECTIVE

View Article Online
View Journal | View Issue

Cite this: *New J. Chem.*, 2014, **38**, 1883

Hollow micro/nanostructured materials prepared by ion exchange synthesis and their potential applications

Chenglin Yan* and Federico Rosei*

Received (in Montpellier, France) 5th August 2013,
Accepted 14th October 2013

DOI: 10.1039/c3nj00888f

www.rsc.org/njc

In recent years there has been a growing interest in synthesizing hollow micro/nanostructure materials using ion exchange methods. This approach was largely enabled by physical and chemical breakthroughs that allowed the reproducible and affordable synthesis of such structures. This *Review Article* aims at summarizing the approaches based on ion exchange methods. It is not intended as a comprehensive coverage of the field, which can in part be found in other excellent reviews, but rather a selection of those contributions that we feel would most help put this emerging field in perspective. Preliminary studies show that the ion exchange method provides a simple and effective route for the synthesis of hollow micro/nanostructures and also results in other complex nanostructures that are challenging to be synthesized by conventional methods. Finally, applications of hollow structures in lithium-ion batteries, photocatalysis, and biomedicine are discussed.

1. Introduction

Functional multi-composite nanomaterials with programmable size and shape are considered potential candidates as building blocks of future nanodevices. To this end, simple and inexpensive techniques for their design, synthesis, tailoring and manipulation are critical.[1–7] Nanostructures with hollow interiors have attractive functional properties, although the complexity of the synthesis often increases as compared to conventional nanomaterials.[8–11] Hollow structures possess interesting features such as low density, high surface-to-volume ratio and low coefficients of thermal expansion and refractive index that make them attractive for

INRS Centre Énergie, Matériaux et Télécommunications, Université du Québec, 1650 Boul. Lionel Boulet, J3X 1S2 Varennes (QC), Canada. E-mail: c.yan@ifw-dresden.de, rosei@emt.inrs.ca

Chenglin Yan

Chenglin Yan received his PhD from Dalian University of Technology in 2008. Thereafter, he joined the Nano(meter)-Femto(second) Lab at the INRS-EMT as a post-doctoral researcher and obtained a prestigious fellowship from FQRNT. In 2010 he moved to the Max Planck Institute of Microstructure Physics in Halle as a Humboldt Fellow. Since 2011 he has been working as a staff scientist and a group leader at the Institute for Integrative Nanoscience at the Leibniz Institute in Dresden where he currently leads a group working on Nanomembranes for Energy Storage. In 2013, the IFW-Dresden awarded Dr Chenglin Yan the "IIN Research Prize 2013" for his group's excellent research work on nanomembrane based energy storage devices.

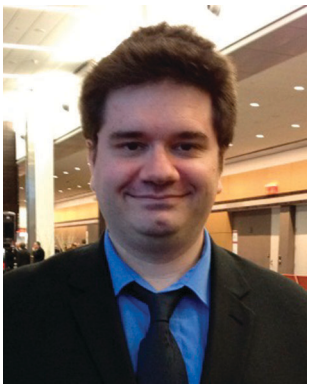

Federico Rosei

Federico Rosei holds the Canada Research Chair in Nanostructured Organic and Inorganic Materials, and is Professor and Director of the Energy, Materials and Telecommunications Centre of INRS in Varennes (QC) Canada. He obtained his PhD in 2001 from the University of Rome "La Sapienza" (Italy). He is Fellow of the American Association for the Advancement of Science, Fellow of the Royal Society of Chemistry (UK), Fellow of the Institute of Physics, Fellow of the Institution of Engineering and Technology, Fellow of the Institute of Materials, Metallurgy and Mining, Fellow of the Institute of Nanotechnology, Senior Member of the IEEE, Fellow of the Engineering Institute of Canada, Member of the Global Young Academy, Fellow of the Australian Institute of Physics, Senior Member of SPIE and Member of the Sigma Xi Society.

applications ranging from catalyst support[10] to chromatography,[11] drug delivery,[12] nanodevices[13] and energy storage.[14] For example, the large fraction of void space in hollow nanostructures has been successfully exploited to control the release of many functional molecules such as drugs, cosmetics and DNA.[15] Likewise, the void space in hollow particles has been used to modulate the refractive index, reduce density, increase active area for catalysis,[10] improve the particles' ability to withstand cyclic changes in volume and expand the array of imaging markers suitable for the early detection of cancer.[12] In addition, several studies have focused on hollow nanostructure electrodes,[16–20] to resolve the problem of rapid capacity fading over extended cycling in lithium-ion batteries.

Until recently, many hollow metal oxides including TiO_2, ZnO, Co_3O_4, SnO_2, MnO_2, CuO/Cu_2O, Al_2O_3–ZnO,[16,21–27] and metal sulfides such as *e.g.* ZnS, CuS, MnS, Sb_2S_3[28–31] have been fabricated through a variety of synthetic methods; the two most widely used approaches to prepare this class of hollow micro/nanostructure materials are hard and soft template syntheses.

Since 1998 there has been a significant increase in research on the template-based synthesis of hollow micro-/nanostructures, originally initiated by Caruso's seminal paper on colloidal template synthesis of hollow spheres.[32] Since this method can be used to fabricate hollow structures from templates of essentially any size, shape and composition, the range of hollow particles available for applications has dramatically expanded.

In the template process, the synthesis of hollow structures usually takes place in three steps, as shown in Scheme 1. The first step is the pre-formation or *in situ* formation of easily removable template materials. The latter are then used as a template for the target coatings to form core–shell structures during the second step. In the last step, by choosing an appropriate etching technique, the inner core is selectively removed from the core–shell structures, forming a hollow structure. The templates can have different compositions and morphologies, for instance silica,[33] polymer,[34–36] or carbon templates,[37] but also vesicles,[38–40] emulsions,[41–43] micelles[44,45] and even gas bubbles[46] have been used. In the hard-template assisted synthesis, anodic alumina membranes were commonly used and the nanostructures were formed on the inner or outer surfaces of the templates using layer-by-layer, sol–gel casting, infiltration, redox reaction, and particle adsorption methods.[32,47–56] In the soft-template assisted synthesis, on the other hand, ionic surfactants as well as nonionic polymeric surfactants were often employed, including gas bubbles produced during the synthetic reactions.[57]

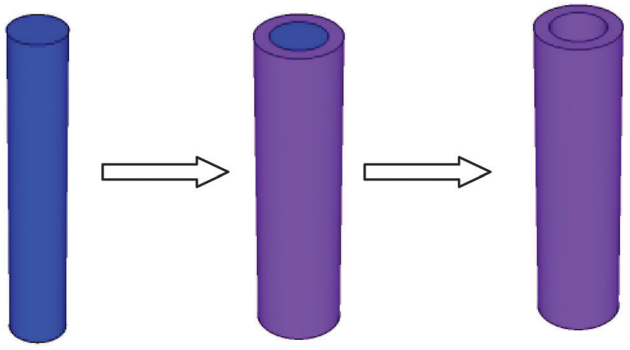

Scheme 1 Schematic illustration of hollow structure formation *via* hard template method.

These advances in synthetic approaches of hollow micro/nanostructured materials have in turn catalyzed applications in a wide range of fields, such as biomedical engineering, catalysis, energy storage and photonics.[10–14] Nonetheless, in the template-assisted approach, non-lithographic preparation of a hard template itself is already a challenging task. In addition, many template materials have high solubility or reactivity and are not stable under strongly acidic or alkaline conditions. For example, the anodic aluminum oxide (AAO) template, widely used for the synthesis of hollow structures, is easily dissolved in basic or acid solutions, making it impractical for this type of synthesis. In some cases, template removal is also challenging. An example of this is the carbon nanotube [CNT] template.[58] Although CNTs are burnable and removable after synthesis, a high-temperature thermal treatment would cause morphological changes of their coatings. Thus, the chemical workability of a template in a specific reactive environment is a crucial selection criterion, even though its shape may fulfil the structural requirement. Another technical barrier associated with the template method is the difficulty in producing particles with a small size because of the intrinsic size limit of the template such as polystyrene or silica spheres. Even though the size can often be controlled by the size of the template, it is challenging to tailor it so as to achieve a very close match for hollow structured materials. Therefore, from a synthesis viewpoint, it is important to develop a range of comprehensive methods, with greater flexibility over the existing template-assisted techniques, to meet new technological requirements. In the following subsections, we focus on the ion exchange synthesis of hollow structured materials.

Insoluble solids that slightly dissociate to give traces of ions in solution can be dissolved with ion-exchangers to produce valuable species. The ion exchange approach has recently been demonstrated to be a simple and versatile method to create a variety of nanostructures.[59–63] In particular, synthesis of nanostructures *via* ion exchange reaction in materials has been shown to be very useful for transforming solid structures into hollow spheres,[61] nanotubes,[62] as well as polyhedral structures.[63] A typical ion exchange reaction occurs between an insoluble solid and a solution during which ions may be interchanged. As shown in Scheme 2, complete transformation of solid $Zn_5(CO_3)_2(OH)_6$ spheres into hollow ZnO spheres at room temperature was achieved simply by mixing $Zn_5(CO_3)_2(OH)_6$ spheres with potassium hydroxide.[61] The formation of hollow structures in such reactions is mainly attributed to the diffusion difference between Zn^{2+} and OH^- in solution, a process analogous to the well-known Kirkendall effect,[64] as well as volume changes. The Kirkendall effect originally refers to the inequality in interdiffusion between brass and copper, and voids are left behind by the more rapidly moving component. The basis of the Kirkendall effect is pore formation caused by the difference in diffusion rates between two species. This strategy has

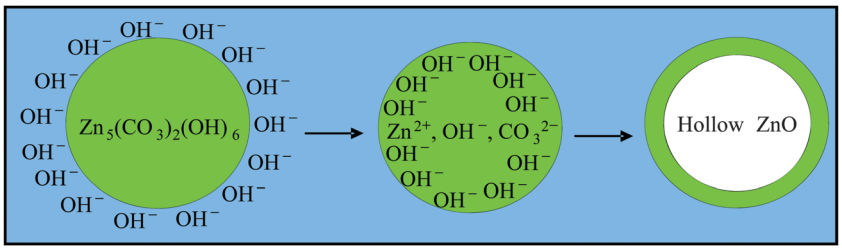

Scheme 2 An ion exchange reaction used for the synthesis of ZnO hollow structures.

also enabled the successful synthesis of a wide range of high quality hollow structures including spheres, tubes and polyhedron structures.[61–63] The Kirkendall effect was first proposed for the formation of hollow Co_3S_4 or CoO nanocrystals by Yin and coworkers,[64] as the authors pointed out that pore formation might initially be induced by the Kirkendall diffusion difference while its later-stage growth may result from other mechanisms such as surface diffusion along the pore walls or a direct escape of core material through gaps in the shells. New directions in the ion exchange synthesis of superlattices, microrings, and hemispheres as well as core–shell structures have been also reported.[61] To obtain more complex structures and control the shape of hollow micro/nanostructure materials as desired, the unraveling and systematic understanding of ion exchange processes is necessary. This review focuses primarily on recent progress in the synthesis of hollow micro/nanostructure materials through ion exchange reactions, with particular emphasis on the current understanding of hollow structure control. Finally, we also briefly discuss the applications of hollow structures in lithium-ion batteries, photocatalysis and biomedicine.

2. Ion exchange synthesis: features

As early as 1799, Berthollet proposed the idea that a chemical reaction should be reversible.[65] Later, Guldberg and Waage proposed that equilibrium is reached in chemical reactions and can be approached from either direction.[66] In 1877 van't Hoff quantified the expression for the equilibrium of a chemical reaction and showed that it is a function of the concentration of the various species involved and that the concentration appears as powers corresponding to the stoichiometric number in the balanced chemical equation.[67]

An ion exchange synthesis is a reaction in which there is an exchange of positive or negative ions between two compounds. These reactions generally take place between two ionic compounds in aqueous solution. The solid is in equilibrium with the slightly dissolved ions of the metal species X and Y, the extent of which is controlled by the solubility product of the solid under a given set of physical conditions. An example is the following:

$$(X^{Z_X})Z_v(Y^{Z_Y})Z_{B(s)} \leftrightarrow Z_Y X^{Z_X} + Z_B Y^{Z_Y} \quad (1)$$

$$K_{sp} = (a_X)Z_Y(a_Y)^{Z_X} \quad (2)$$

where a_X and a_Y are the activities of species X and Y in solution and K_{sp} the solubility product of the solid. The sp subscript indicates the solid phases and Z the valences of the species. In the case of $CaCO_3$, X and Y represent Ca^{2+} and CO_3^{2-} respectively with $Z_X = Z_Y = 2$. The relationship between concentration and thermodynamic force in a chemical reaction or simple transformation is one of the most important in thermochemistry. It is important to recognize that this driving force results from maximizing entropy and therefore, minimizing the Gibbs energy and naturally leads to the concept of equilibrium. The relationship between equilibrium conditions and concentration originates from the definition of the Gibbs energy or chemical potential.

From eqn (2) it follows that K_{sp} is a function of the solubility product of the solid and the thermodynamic equilibrium constant of the ion exchanger. For monovalent–monovalent exchange of species, the thermodynamic dissolution constant defined by eqn (2) becomes the product of the solubility and thermodynamic equilibrium constant. When two electrolytic solutions are combined, a precipitate may or may not form. To determine whether or not an ion exchange reaction will take place, two factors should be examined. First, determine the possible combinations of ions that could result when the two solutions are combined to see if any of them are deemed "insoluble" based on solubility tables. Second, determine if the ion concentrations are high enough so that the reaction quotient exceeds the K_{sp} value. In addition, there is a dilution of all species present that must be taken into account. In the ion exchange reaction, the dissolution of the insoluble solid can further be enhanced if a precipitate is formed between the counter ion that initially saturates the ion exchange resin and the co-ion initially in the solid.

2.1. Ion exchange synthesis as a general route to micro/nano structured materials

As one of the widely used routes to growing micro/nanomaterials, the direct precipitation method permits minute control over shape and size due to rapid precipitation under high supersaturation. The use of a simple ion exchange reaction has been shown to be an effective method offering a better control of shape and size with respect to the direct precipitation reaction.

Yan and co-workers developed an ion exchange reaction for the synthesis of Mn_2O_3 nanomaterials.[60] As shown in Fig. 1, the strategy described herein is derived from the solubility difference between two carbonate salts $(Mg_5(CO_3)_4(OH)_2$ and $M_x(CO_3)_y(OH)_z)$, in which metal cations can be driven from one liquid phase into one solid phase in the solution system. The resulting metal carbonate salts were initially formed and

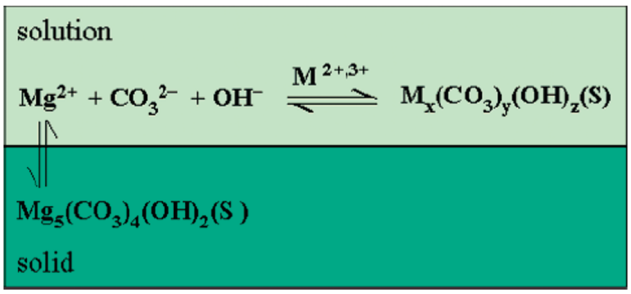

Fig. 1 General spontaneous ion replacement process in an aqueous solution. M represents metal ions and *x*, *y*, *z* are valence states. Reproduced with permission from ref. 60, copyright 2006 American Chemical Society.

subsequently calcined to form highly crystalline metal oxides. This is because the K_{sp} coefficient for $Mg_5(CO_3)_4(OH)_2$ is higher than that of $M_x(CO_3)_y(OH)_z$ under the same solution conditions, which implies a tendency for the reaction to progress toward the target samples, with the chemical equilibrium moved to the right side. Using this strategy, Mn_2O_3 cubes were obtained by the calcination of a precursor, which was synthesized by the ion exchange reaction of Mg^{2+} with Mn^{2+} between $MnSO_4$ and $Mg_5(CO_3)_4(OH)_2$ in solution at room temperature. Scanning electron microscopy (SEM) images (Fig. 2) of Mn_2O_3 cubes show that they form regular cubic shapes. Higher magnification images revealed that the synthesized cubes had a uniform edge length of around 800 nm.

From an experimental point of view, a suitable amount of metal ion added to the reaction solution and a high reaction temperature are required to obtain pure-phase metal oxide nanomaterials. As a result, reaction in a solution phase at an elevated temperature was more favorable than a room-temperature

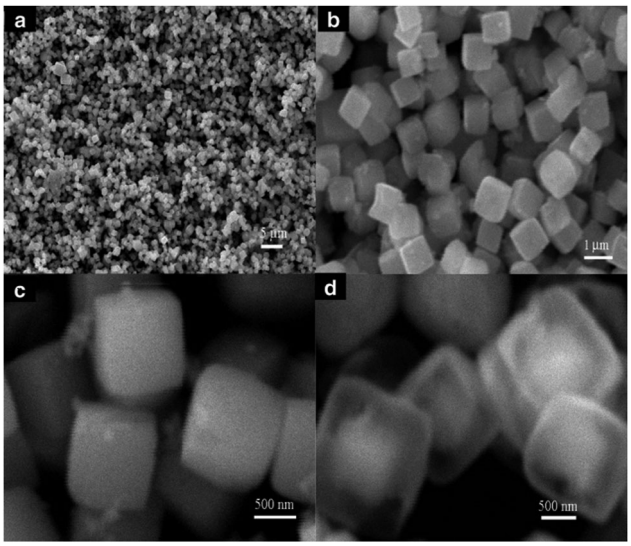

Fig. 2 SEM images of Mn_2O_3 and $MnCO_3$ cubes. (a–c) SEM images of monodispersed and well-shaped Mn_2O_3 cubes obtained by calcination of $MnCO_3$ at 600 °C. (d) $MnCO_3$ cubes synthesized by the ion replacement reaction in the presence of surfactant. Reproduced with permission from ref. 60, copyright 2006 American Chemical Society.

reaction since the supply of metal ions was constant and sufficient under the former conditions. In principle, the high efficiency of the ion exchange reaction can be extended more broadly to exchange reactions with other ion systems, providing new or complementary synthetic routes to a variety of materials. Yan *et al.* have shown that the above strategy could be extended to other functional metal oxides such as ZnO, CuO, CdO, Al_2O_3, and CaO.[60] This synthetic approach also allowed further reduction of the growth temperature to room temperature, leading to the development of an effective, low-cost fabrication process with good potential for scale up.

The efficiency of the ion exchange reaction as a synthetic method ultimately depends on the thermodynamic driving force and the activation barrier. To employ ion exchange as a versatile synthetic method for nanomaterials, it will be important to understand and control the factors that affect the kinetics and thermodynamics of the reaction other than temperature and ion concentration.

2.2. Application of ion exchange synthesis to prepare hollow structured materials

Due to the structural precision and wide availability of hollow nanostructured materials, the ion exchange reaction can result in well-defined and uniformly-sized hollow materials and the framework of the starting materials can be preserved during the ion exchange process. For instance, the complete transformation of CdSe into Ag_2Se hollow nanocrystals was achieved simply by mixing a CdSe nanocrystal solution with a silver salt solution at room temperature.[68] The fast kinetics and ion exchange rate of the reaction were considered to be mainly due to the lower activation barrier for the diffusion of atoms in nanocrystalline solids compared to the bulk phase.[68] Both cation and anion exchange reactions have been extensively employed for the synthesis of a variety of hollow structured materials. Konenkamp demonstrated that certain cations (*e.g.* Ag^+, Sb^{3+}, Bi^{3+}, and Cu^+) can be used to replace Cd^{2+} in thin films.[69] A complete replacement of the original compound was achieved through the exchange of the metal ions. In most cases this replacement is accompanied by a change in crystal structure and stoichiometry. Under these conditions the morphology of the structure was found to depend sensitively on the processing route. Columnar and tubular films of Ag_2S, Cu_2S, Bi_2S_3, or Sb_2S_3 were prepared from columnar ZnO films.[70–74] With respect to anion exchange, Wang and co-workers reported the transformation of columnar ZnO into tubular ZnS by exposure to H_2S gas.[75] The conversion of ZnO into ZnS nanotubes occurred in solution and was formed by a direct reaction of H_2S with the surface layer of ZnO in the presence of water. Subsequent work indicated that the formation of nanotubes through anion exchange reaction is possible if the Zn^{2+} and OH^- from water are mobile in the solution, so that they can diffuse through the porous ZnS wall and combine with the H^+ and S^{2-} ions, resulting in the formation of empty tubular structures.

During ion exchange reactions for the production of hollow structures, the structural difference between precursors and product phases is the most easily quantifiable factor and bears

additional importance concerning the change in nanocrystal morphology after the reaction. Understanding the factors that affect the activation barrier is a challenging undertaking. The activation barrier for diffusion and exchange of cations depends on many factors, such as the structure of the ion sublattice, the ionicity of the cation–anion interaction and the structural difference between the precursors and product phases. A change in nanocrystal morphology, especially when the reaction involves a large change in the volume or lattice parameters, can be an important issue when the initial reactant nanocrystals are used as structural template. Son and coworkers proposed that the observed changes in size can be accounted for by changes in the crystal unit cell symmetry and lattice parameters during the ion exchange reaction.[68] This occurs because the structures of Se^{2-} sublattices in wurtzite CdSe and various phases of Ag_2Se were investigated to show the topotaxial relationship between the reactant and product phases and associated changes in dimension.

2.3. Ion exchange synthesis coupled with redox reaction

In addition to the ion reaction without valence variation, the ion exchange process can also be combined with the well-established redox reaction developed[76–78] to add new functions to ion exchange synthesis. For instance, it is feasible to convert CuCl nanorods into CuS nanotubes where Cu^+ cations in CuCl were partly oxidized to Cu^{2+} by S^{2+} during the ion exchange reaction process.[76] In CuS, there exist both univalent and divalent copper cations.[77,78] The oxidation state of copper in CuCl is +1, therefore, the transformation of CuCl nanorods to CuS nanotubes through ion exchange should involve a redox reaction. In this process, the inner part of the CuCl rod was consumed gradually and a CuS nanotube was formed *via* an oxidation reaction when the transport rate for Cu atoms through the copper sulfide layer was much faster than S atom transport through the copper sulfide layer in the opposite direction. Some hollow structures have been obtained by ion exchange synthesis coupled with a redox reaction. Ye *et al.* demonstrated the growth of micrometer-scale MoS_2 hierarchical hollow cubic cages assembled by bilayers through a coupled redox reaction.[79] These MoS_2 cages can be electrochemically charged and discharged with a high capacity of 375 mA h g^{-1} due to the more active edges exposed on the upright-standing nanoplates. Similarly, a hollow octa-18-face polyhedron, and octa-rhombododecahedron, and rhombododecahedron were recently fabricated through the controllable synthesis of surfactant–molybdate composite precursors.[80] The method was extended to other sulfide systems and the synthesized materials could be potentially used for device applications with surfactant/inorganic $[(C_4H_9)_4N]_{0.4}(MoO_{2.8})$ combination.

3. Ion exchange synthesis of hollow micro/nanospheres

3.1. Metal oxide hollow spheres

The potential of the ion exchange reaction[60] can be fully exploited for the synthesis of metal oxide hollow spheres with the same diameter as their precursors by using microspheres as a reactive template. This is an important advantage because metal oxides represent an emerging class of materials, with important structure-related properties including superconductivity, photovoltaic conversion, catalytic activity, magnetism and gas sensitivity.[81–86]

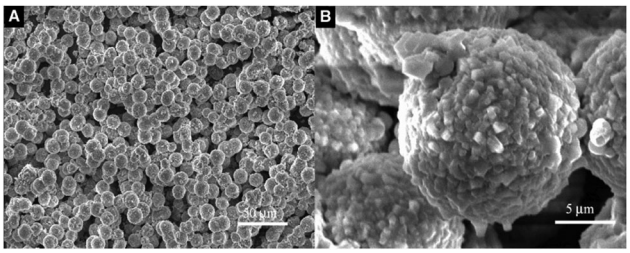

Fig. 3 SEM images of the spherical $Zn_5(CO_3)_2(OH)_6$ with a hierarchical structure composed of nanocubes by the solvothermal reaction for 4 h: (A) morphology of the monodispersed samples; (B) detailed view on an individual microsphere composed of nanocubes. Reproduced with permission from ref. 62, copyright 2006 American Chemical Society.

Fig. 3 displays SEM images of $Zn_5(CO_3)_2(OH)_6$ microspheres with a uniform size and morphology as the precursors for the subsequent ion exchange reaction. To succeed in converting the filled $Zn_5(CO_3)_2(OH)_6$ microspheres into hollow ZnO microspheres, the as-prepared spherical $Zn_5(CO_3)_2(OH)_6$ powders were directly added to the KOH solution and subsequently kept aging for ~8 hours at room temperature. The results for the conversion of filled $Zn_5(CO_3)_2(OH)_6$ microspheres to hollow ZnO microspheres are displayed in Fig. 4.

The hollow ZnO microspheres form over a reaction time of 4–36 h. Some broken pieces of hollow shells are also observed. A high magnification image indicates that the surface of hollow microspheres exhibits a porous structure (Fig. 4C), with diameter similar to $Zn_5(CO_3)_2(OH)_6$ microspheres (Fig. 3).

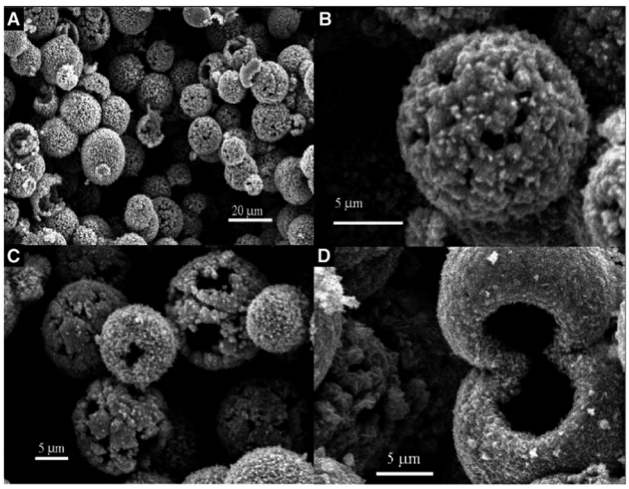

Fig. 4 SEM images of the as-synthesized hollow ZnO microsphere by the room-temperature treatment of $Zn_5(CO_3)_2(OH)_6$ microspheres in the KOH solution: (A) overall product morphology; (B) and (C) detailed view on the surface of hollow ZnO microspheres; (D) twin hollow ZnO microspheres. Reproduced with permission from ref. 62, copyright 2006 American Chemical Society.

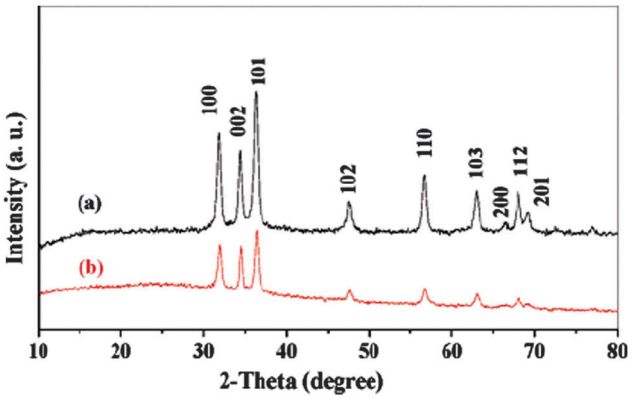

Fig. 5 XRD patterns of hollow ZnO samples synthesized from $Zn_5(CO_3)_2(OH)_6$ by different synthetic route: (a) calcination of precursor at 400 °C and (b) ion exchange synthesis. Reproduced with permission from ref. 62, copyright 2006 American Chemical Society.

The ion transformation was followed using X-ray diffraction (XRD), as shown in Fig. 5. The XRD pattern taken from the ZnO sample can be assigned to the hexagonal lattice of ZnO, with lattice constants a = 3.249 Å and c = 5.206 Å. No peaks assigned to the $Zn_5(CO_3)_2(OH)_6$ precursors were detected, indicating a complete ion exchange between $Zn_5(CO_3)_2(OH)_6$ and OH^-. All $Zn_5(CO_3)_2(OH)_6$ peaks disappeared after the ion exchange conversion. Calcination of $Zn_5(CO_3)_2(OH)_6$ microspheres at 400 °C also results in the formation of ZnO (Fig. 5a), with a similar solid structure.

The unique feature of the above employed ion exchange route lies in the fact that the sizes of the products are determined by the size of the starting spheres and the balance between the density and molar volume of $Zn_5(CO_3)_2(OH)_6$ relative to ZnO. ZnO is a widely used to direct wide-band-gap semiconductor with the highest E_g = 3.6 eV among all II–VI compounds. It is being widely studied with the aim of optimizing its optical properties by tailoring its shape and size.[87–90] In addition, hollow ZnO microspheres may have promising applications in filters, microreactors and catalyst carriers due to their unique hollow features with a high surface area and high porosity.[91]

In addition to solution-phase conversion based on ion exchange reactions, gas-phase reactions are also incorporated for carrying out this chemical conversion method. To illustrate this concept, we describe a specific example from Xue's group.[92] The authors first synthesized solid precursors of CuS microspheres; the reaction of CuS spheres with oxygen from air at 700 °C led to the formation of porous CuO hollow microspheres. Upon heating the precursor structures in air, a layer of copper oxide initially developed into a shell on the surface as the copper sulfide oxidized. Oxygen from air was still able to diffuse through this shell, so the oxidation continued during heating. However, the copper sulfide diffuses outwards faster than the copper oxide shell can diffuse inwards, leaving a cavity at the center of the structures. The high porosity of the resulting shell structures was a result of the release of sulfur dioxide from the objects, coupled with volume loss arising from conversion from sulfide to oxide. The holes created by these processes yield porous shells. Xue and co-workers subsequently extended this strategy using precursors of nickel sulfide, cobalt sulfide and copper sulfide, and obtained various metal hollow structures.[92,93] For example, CuO hollow structures (Fig. 6b–d) can be synthesized using Cu_2S as precursor (Fig. 6a). The obtained porous and hollow CuO architectures possess high thermal stability as the products were synthesized at a relatively high temperature of ~700 °C. The apparent advantages of as-prepared hollow structures in providing more surface area for increasing reactive sites and better mechanical stability make them suitable for many important applications in energy storage, such as lithium-ion batteries and catalysis.[12,14]

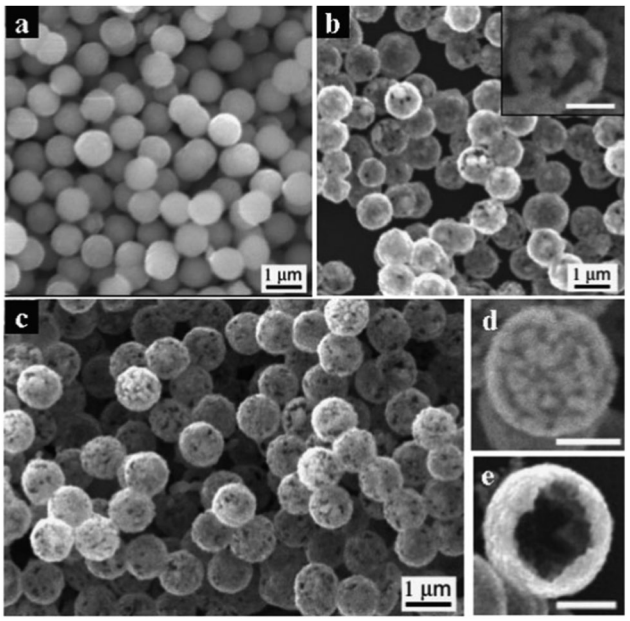

Fig. 6 SEM images of Cu_2S precursor particles and their conversion into CuO products at different reaction stages, summarizing all major morphological changes involved in non-equilibrium interdiffusion, volume loss, and gas release: (a) monodisperse spherical Cu_2S precursor, and (b–e) formation of porous CuO hollow spheres by complete oxidation of Cu_2S after reaction. Reproduced with permission from ref. 92, copyright 2008 Wiley-VCH Verlag GmbH & Co. KGaA.

3.2. Metal sulfides hollow micro/nanospheres

Chalcogenide semiconductor nanocrystals have unique shape- and size-dependent physical and chemical properties that differ drastically from their bulk counterparts.[94–96] These nanocrystals find potential applications in various fields such as solar cells, electrical, optical and magnetic devices, biological labeling and diagnostics, hydrodesulfurization and hydrogenation catalysts.[97–103] In particular, hollow metal sulfides are attracting great attention in both theoretical studies and for practical application, due to their properties as a consequence of their large number of surface atoms and the three-dimensional confinement of electrons.[104]

The shape transformation from CdS hollow spheres to larger Ag_2S hollow spheres by ion exchange reaction was shown to be an efficient route to synthesize hollow metal sulfide structures.[68]

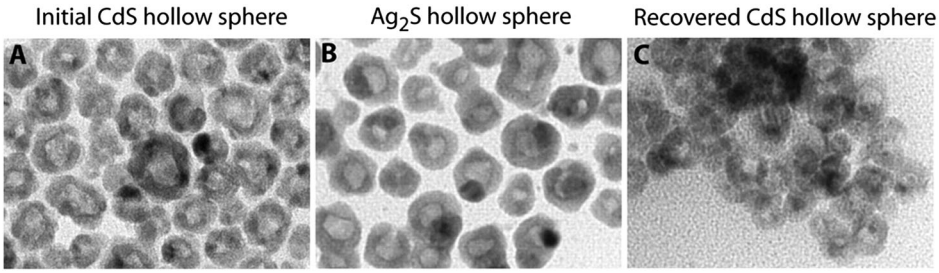

Fig. 7 (A to C) TEM images of (A) initial CdS hollow spheres, (B) Ag_2S hollow sphere produced from cation exchange of CdS, and (C) recovered CdS from the reverse cation exchange reaction. From ref. 68, copyright 2004 reprinted with permission from AAAS.

Ag_2S hollow spheres were formed by mixing CdS hollow spheres with $AgNO_3$ solution in a slightly larger amount than necessary to replace all the Cd^{2+} ions in the nanocrystals, as shown in the transmission electron microscopy (TEM) image of Fig. 7A. CdS hollow spheres maintain their general morphology during the cation exchange, although a smoothing of the rough surface and a small increase in volume were observed. The authors also claimed that other even more complex and high-energy nonequilibrium shapes of nanocrystals, such as hollow spheres and branched tetrapods, can be obtained through complete cation exchange reaction if the size of the staring materials is greater than 5 nm (Fig. 7). Therefore, the ion exchange method not only provides a simple and effective route for the synthesis of hollow structures, but can also be used to prepare other complex nanostructures that are challenging to be produced by conventional methods. In the case of CdTe tetrapods, a slight expansion (about 5%) of the width of each branch was observed after the transformation to Ag_2Te. This kind of cation exchange reaction was often carried out in aqueous solution containing the respective salt precursors. In these reactions, a large difference in solubility provides the driving force for ion replacement. Generally, the starting hollow material present in a solution containing an appropriate precursor ($AgNO_3$ solution) will spontaneously undergo ion exchange to yield the product with a lower solubility and similar hollow structures (Ag_2S). On the other hand, when the solubility of the desired product is higher than that of the precursor material, new strategies are needed to drive the ion exchange reaction.

3.3. Metal selenide hollow micro/nanospheres

As important functional semiconductors, metal selenides have been widely studied[105–112] because of potential applications in areas such as solar cells, sensors, infrared detectors and photovoltaics.[113–116] A generalized chemical conversion approach for the synthesis of hollow metal selenides has been recently developed through an ion exchange reaction.[117,118] Li and coworkers reported the use of hollow microspheres of an active semiconductor (*e.g.* ZnSe) as a starting reactant to synthesize a number of hollow selenide microspheres with lower K_{sp} values.[117] Fig. 8a displays the XRD patterns of Ag_2Se and $Cu_{2-x}Se$ microspheres prepared at room temperature and CdSe microspheres synthesized at 140 °C. The patterns demonstrate that all three are pure-phase selenides. For the $Cu_{2-x}Se$

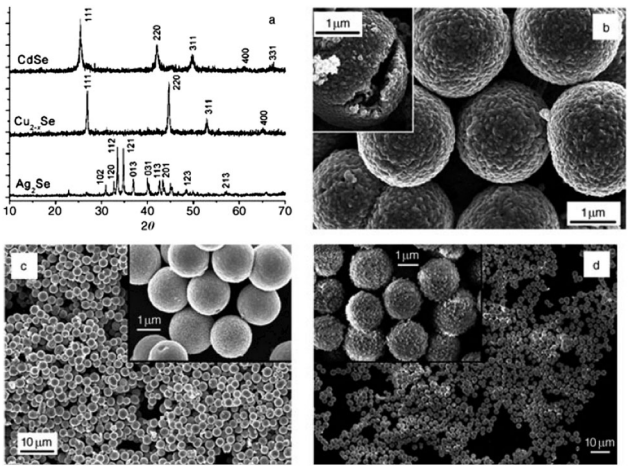

Fig. 8 XRD patterns (a) and SEM images of Ag_2Se (b), $Cu_{2-x}Se$ (c), and CdSe (d) microspheres prepared by using ZnSe as the precursor based on ion exchange reaction. Reproduced with permission from ref. 117, copyright 2005 Wiley-VCH Verlag GmbH & Co. KGaA.

and CdSe products, cubic structures were ''inherited'' from the original ZnSe templates due to the mild reaction conditions. Fig. 8b–d report SEM images of as-prepared Ag_2Se, $Cu_{2-x}Se$, and CdSe products, respectively (the insets of Fig. 8c and d are high-magnification images of $Cu_{2-x}Se$ and CdSe microspheres, respectively). The products still maintain a spherical morphology. Compared to the original ZnSe microspheres, they exhibit a relatively rough surface and a similar diameter. The inset of Fig. 8b shows an individual cracked Ag_2Se sphere, indicating that these spheres also 'inherit' the framework from the ZnSe microspheres.

Metal selenides were obtained with K_{sp} values that were very close to or only a little lower than that of ZnSe (*e.g.*, CdSe, CoSe, and NiSe); however, high ionic concentrations and additional energy is required to successfully complete the conversion reaction. For heavy metal ions such as the aforementioned Ag^+, Cu^{2+}, Pb^{2+}, and Hg^{2+}, whose selenides have K_{sp} values that are significantly lower than that of ZnSe, Ag_2Se and $Cu_{2-x}Se$, a fast ion exchange reaction can be expected, in which less than one second is needed to obtain the final hollow structures.

A similar growth process for metal selenide hollow spheres with core–shell structures through ion exchange reaction was reported by Xia and co-workers.[118] Starting from a Se@Ag_2Se

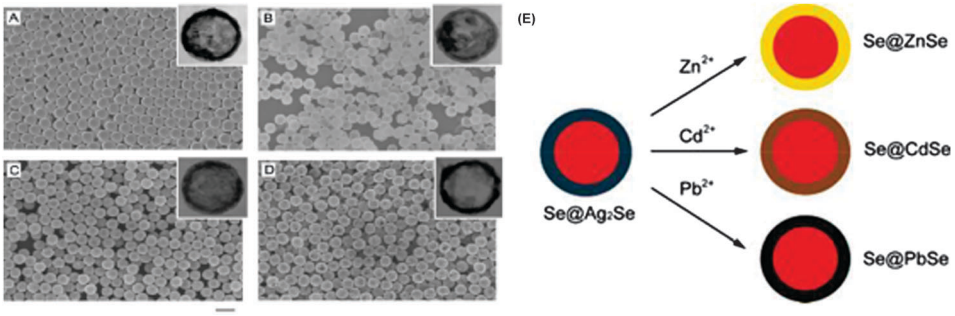

Fig. 9 SEM images of (A) Se@Ag_2Se, (B) Se@ZnSe, (C) Se@CdSe, and (D) Se@PbSe colloidal spheres. (E) Schematic showing the synthesis of core–shell colloidal spheres *via* cation exchange reactions. Reproduced with permission from ref. 118, copyright 2007 American Chemical Society.

precursor (Fig. 9), hollow Se@ZnSe, Se@CdSe, and Se@PbSe spheres were prepared through exchange reactions with Zn^{2+}, Cd^{2+} and Pb^{2+}. All metal selenide samples display a spherical shape and similar diameter and exhibit a monodisperse size distribution and smooth surface (Fig. 9E). This is a unique feature, as it allows for the synthesis of semiconductor colloidal spheres with the same size but different compositions. It is particularly significant because it also implies that it is feasible to further increase the diversity of cations that can be used in the cation exchange of a colloidal system to produce multi-functional core–shell spheres with a variety of properties.

4. Ion exchange synthesis of nanotubes

In recent years, considerable attention has focused on nanotubes[119–123] due to their unique structure related properties and range of potential applications.[124–131] The formation of tubular nanostructures typically requires layered, anisotropic, or pseudo-layered crystal structures.[132–135] This represents a challenge because inorganic compounds usually do not exhibit such structures. Inorganic nanotubes with non-layered structures are less well studied than CNTs, in part due to difficulties in controlling their dimensions and shapes.[129–131,136] However, inorganic nanotubes share many advantages of CNTs and can match the emerging demands for various functionalities. The properties of such non-carbon materials[137] are of great interest due to their improved functionalities compared to colloidal or other forms of titania for applications in photocatalysis,[138,139] sensing[140] and photovoltaics.[141,142] The successful synthesis of hollow structured microspheres through the ion exchange reaction indicates that this synthetic approach could be extended to preparing hollow structured nanotubes by selecting a proper ion exchange process.

4.1. Nanotubes prepared by using metal oxide as the precursor

As reported by Alivisatos and co-workers, excess Cd^{2+} ions and a small amount of tributylphosphate (TBP) are required to enable the exchange between Cd^{2+} and Ag^{+} in nanocrystals.[68] This method was recently shown to be extendable to the synthesis of ZnS nanotubes with an addition of a small amount of thioglycolic acid in the Na_2S solution, using ZnO nanorods as precursors.[61] In this case, thioglycolic acid plays a pivotal role as it can bind to Zn^{2+} ions in the shells of ZnO nanorods in solution, forming intermediate complexes. The stronger interaction between thioglycolic and Zn^{2+} allows the association of Zn^{2+} from ZnO nanorods, leading to the formation of ZnS shell on their surface through the ion exchange reaction. Heating (to around 120 °C) was necessary to facilitate this process.

The precursor ZnO is shown in Fig. 10; all samples display a rod shape and are characterized by a smooth surface. ZnO nanorods align approximately normal to the zinc substrate with a diameter of about 200 nm and a thickness of about 4 μm. When ZnO nanorod arrays are introduced into the $HSCH_2COOH$ and Na_2S solution, the formation of $ZnHS^{+}$ complex between the lone pair electrons in the sulfur atom of $HSCH_2COOH$ molecule and the vacant d orbital of the Zn^{2+} ions leads to an increase in the activity of Zn^{2+} ions on ZnO nanorods and then ZnS nucleates by dissolution of ZnO nanorods in the Na_2S solution. After the reaction, ZnO–ZnS core–shell nanowires are obtained.

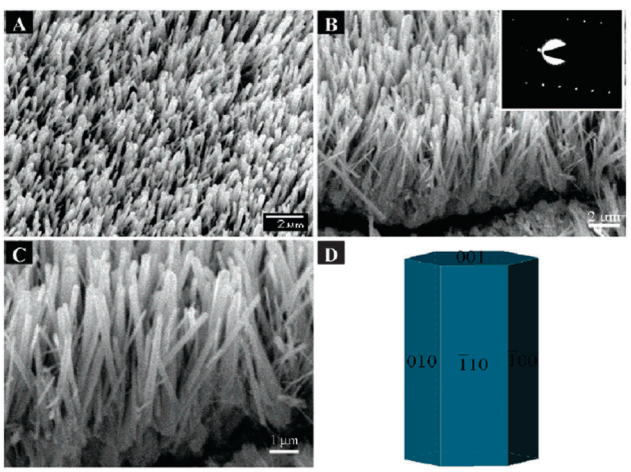

Fig. 10 SEM images of ZnO nanorod arrays grown on the zinc foil substrate at 120 °C: (A) tilt view; (B) edge tilt view (the inset is the corresponding SAED pattern); (C) a high-magnification image of ZnO nanorod arrays; (D) crystal growth habit of wurtzite ZnO nanorods. Reproduced with permission from ref. 61, copyright 2006 American Chemical Society.

Since ZnO is an amphoteric oxide, KOH solution was used to treat ZnO–ZnS core–shell nanowires, leading to the dissolution of ZnO cores and finally ZnS nanotube arrays are obtained. The recent successes of the anion exchange reaction for the synthesis of hollow structures has greatly broadened the scope of ion exchange reactions. During the ion exchange reaction, normally the diffusion rate of cations controls the final morphology as the diffusion rate of cations is normally much faster than the diffusion of anions, therefore, faster diffusion of O^{2-} than incoming S^{2-} results in the formation of a hollow structure from the anion exchange reaction.

As shown in Fig. 11, a partial conversion of the ZnO nanorods and etching in KOH results in free-standing ZnS tubes with open ends and a pore size of about ~400 nm. The inset of Fig. 11A displays a high-magnification SEM image of a ZnS nanotube, showing a perfect hexagonal shape. The selected area electron diffraction (SAED) pattern of the chosen ZnS nanotube (shown in the inset of Fig. 11B) indicates that the structures are polycrystalline. Energy dispersive X-ray (EDX) spectroscopy was used to confirm the local chemical composition of ZnS nanotubes. The EDX spectrum showed strong peaks of only Zn and S elements, indicating that pure ZnS nanotubes can be successfully obtained by the KOH treatment of ZnO–ZnS core–shell nanowires. The geometrical model of ZnS nanotube arrays provides clear evidence of tube shaped structures (Fig. 11D). To control the size of the target semiconductor hollow microspheres, the diameter of the starting ZnO nanorods with a relatively large K_{sp} value must be controlled.

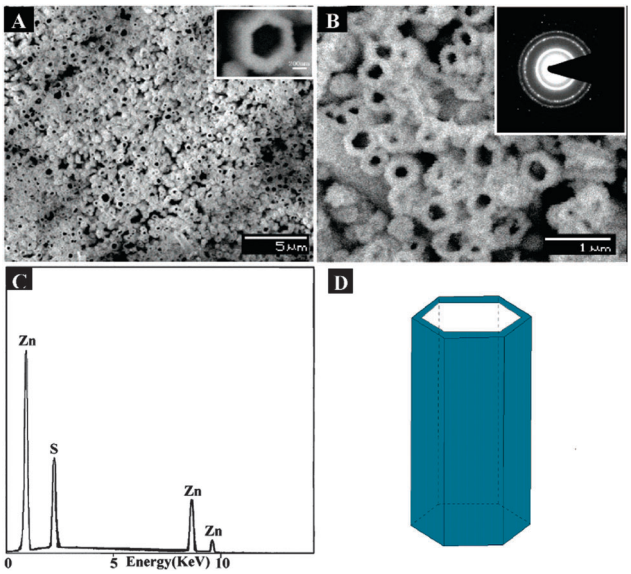

Fig. 11 (A and B) SEM images of ZnS nanotube arrays (the inset of Fig. 11A is a magnified image of ZnS nanotubes and the inset of figure (B) is the corresponding SAED pattern). (C) EDX spectrum taken from the surface of ZnS nanotube arrays. (D) The geometrical model of ZnS nanotube. ZnO nanorod arrays were used as a template for the fabrication of ZnO/ZnS nanocables by sulfurization of ZnO after a thioglycolic acid-assisted reaction. Reproduced with permission from ref. 61, copyright 2006 American Chemical Society.

These features are reproducible and routinely achievable for all the samples described in this review.

4.2. Nanotubes prepared by using metal salts as the precursor

As-synthesized zinc salt ($Zn_5(CO_3)_2(OH)_6$) nanowires were shown to yield, upon ion exchange reaction, ZnO nanostructures with modified morphologies such as hollow nanotubes. The morphological change is derived, in this case, from directional material flows due to different diffusivities for the reacting atomic species. The methodology has since been used to yield nanostructures with various compositions and shapes.[62]

To produce $Zn_5(CO_3)_2(OH)_6$ nanowire precursors with reduced sizes and improved monodispersity, the synthesis was performed using a modification of the hydrothermal process in a homogeneous reaction system. Urea has been recently reported as a neutralizing agent for the homogeneous hydrolysis of aqueous solution of metal acetates.[143–146] The lower hydrolysis rate allows for a better control of the precipitation conditions resulting in the formation of a uniform and well-defined morphology. The decomposition of urea at ~80 °C produces hydroxide anions and carbonate anions, and $Zn_5(CO_3)_2(OH)_6$ nanowires can be formed through the reaction of Zn^{2+}, OH^- and CO_3^{2-}. Rapid formation of nanowires upon reaction was indicated by the originally colorless solution producing gas bubbles of CO_2 and NH_3. The transformation of solid nanowires into hollow ones was performed through the ion exchange reaction between $Zn_5(CO_3)_2(OH)_6$ and S^{2-} from thioacetamide, which can react with water at a high temperature to produce H_2S. ZnS particles were thus formed as a result of the reaction between $Zn_5(CO_3)_2(OH)_6$ and H_2S in solution.

During the structural transformation from $Zn_5(CO_3)_2(OH)_6$ nanowires into ZnS nanotubes, the reaction was surface mediated by organic molecules so that the voids were observed to grow horizontally along the wire axis (Fig. 12a). This is related to a controlled preferential adhesion of H_2S produced by the decomposition of thioacetamide at high temperature of ~200 °C. Hence, the high concentration of H_2S gas dissolved in solution at the nanowire surface promotes the diffusion of Zn^{2+} along the longitudinal axis, leading to the observed anisotropic growth of vacancies. This method represents a different strategy

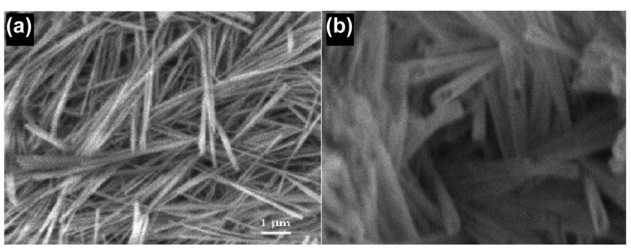

Fig. 12 SEM images of $Zn_5(CO_3)_2(OH)_6$ nanowires (a) by the hydrothermal reaction and their conversion to ZnS nanotubes (b). Part (a) is reprinted with permission from ref. 146. Part (b) is reprinted from C. Yan, D. Xue, L. Zou, A solution-phase approach to the chemical synthesis of ZnO nanostructures *via* a low-temperature route, *Lancet*, 2008, **453**, 87–92, copyright (2008), with permission from Elsevier.

of applying the ion exchange reaction to nanotube synthesis from the one presented in Fig. 12b.

The ion exchange reaction at the solid/liquid interface can easily be extended to exchange with other anions. For instance, ZnS nanocrystals may be transformed into ZnSe and ZnTe hollow structures through the anion exchange reaction with a solution containing Se or Te ions, respectively, under a specific reaction temperature. On the other hand, attempts to induce cation exchange could also be an alternative method for the synthesis of other metal oxide nanomaterials with hollow structures under similar experimental conditions,[147–149] as long as there is a solubility difference between the reactant and the product.[150–153]

4.3. Nanotubes prepared by using metal sulfides as the precursor

Metal sulfides have great potential for use as precursors for the ion exchange synthesis of metal sulfide and selenide hollow structures due to their higher solubility with respect to metal oxides.[117,154] By introducing $HgCl_2$ into the aqueous dispersion of CdS nanotubes under stirring, HgS nanotubes were formed through cation exchange due to the difference of solubility product constants between HgS ($K_{sp} = 1.6 \times 7 \times 10^{-52}$) and CdS ($K_{sp} = 87 \times 10^{-27}$).[154] The resulting HgS nanotubes have a cubic structure. The synthesis of CdS nanotubes was performed as follows. Cd–TGA nanowires were first prepared in the presence of poly(acrylic acid) sodium salt (PAA). The mercury salt was added to the above CdS colloid solution, followed by readjustment of the pH to 7.0. This procedure resulted in the substitution of the surface Cd^{2+} ions by Hg^{2+} ions. The precipitation of Cd^{2+} ions by adding Na_2S or H_2S leads to colloidal particles consisting of a CdS core surrounded by a monolayer of HgS and almost one monolayer of CdS as the outermost shell. The thickening of the HgS layer was simply achieved by repeating the substitution and re-precipitation steps.

4.4. Nanotubes prepared by metal polymer as the precursor

Metal polymers (coordination chains) containing metal cation centers linked by ligands can lead to the formation of numerous 1D, 2D and 3D coordination polymers with unique structures, which can be used as template to direct the formation of various nanostructures. Some isolated single coordinate chains with distinct 1D structures and even bundles can be formed in solution through interchain interactions.[155–158] Therefore, isolated 1D metal polymers or chain bundles could be expected to act as a new type of precursor for the synthesis of tubular structures through ion exchange reactions. The aforementioned inorganic precursors such as metal oxides, metal salts and metal sulfides were generally preferred as starting materials in fabricating hollow nanostructures. In this section, a metal thiolate polymer is reported as the starting material for the synthesis of CdTe nanotubes based on the ion exchange reaction. This may provide a new precursor to synthesize hollow nonspherical structures due to the abundant morphologies of metal polymers. Gao and co-workers synthesized CdTe nanotubes based on the metal polymer Cd–thioglycolic acid (Cd–TGA) as the precursor (Fig. 13).[154]

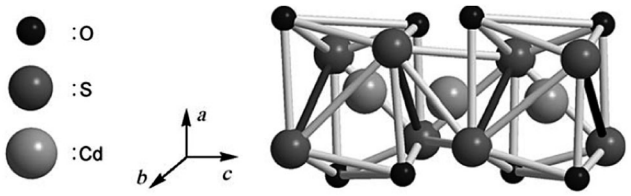

Fig. 13 Illustration of the possible coordination structures in one-dimensional Cd–TGA. Reproduced with permission from ref. 154, copyright 2006 Wiley-VCH Verlag GmbH & Co. KGaA.

Upon introduction of NaHTe, the aqueous dispersion of the metal polymer Cd–TGA nanobelts can be converted into the CdTe nanotubes through exchange of Cd^{2+} ions. TEM imaging (Fig. 14) demonstrated that the inner and outer diameters of the nanotubes were in the ranges of 12–20 nm and 30–50 nm, respectively. The SAED pattern of the nanotubes indicated that

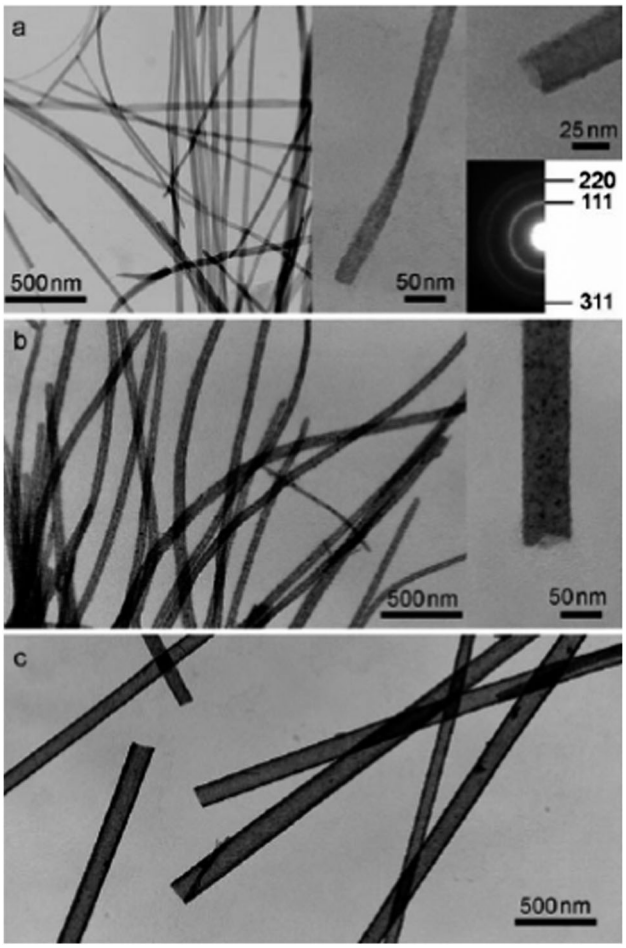

Fig. 14 TEM images of CdTe nanotubes obtained by introducing NaHTe into the aqueous dispersions at different solution conditions: (a) in the absence of PAA, (b and c) in the presence of PAA using Cd/TGA/AA molar rations of 1 : 1 : 0.1 (b) and 1 : 1 : 0.3 (c), AA is the repeat unit of PAA. The insets show TEM images taken under higher magnifications as well as an electron diffraction pattern of the nanotubes presented in part (a). Reproduced with permission from ref. 154, copyright 2006 Wiley-VCH Verlag GmbH & Co. KGaA.

the CdTe adopted a cubic structure. The length of these tubes was typically hundreds of micrometers, quite similar to the initial length of the precursors. The authors also proposed an ion exchange mechanism, which included three key points: (a) CdTe nanocrystals were formed on the surface of the precursor nanobelts by an anion-exchange reaction resulting from the lower solubility of CdTe in solution; (b) self-assembly of CdTe nanocrystals results in the formation of a CdTe nanotube on the surface of the precursor nanowire; (c) this nanotube structure expands at the expense of the precursor nanowire. The authors further extended this strategy to the synthesis of CdS nanotubes, by introducing Na_2S instead of NaHTe into an aqueous dispersion of the precursor sample.

By using a similar precursor ($HSCH_2CH(NH_2)COO$–Pb–OH nanowires), Zhu's group also demonstrated the synthesis of very high-quality ultrathin lead chalcogenide (PbE, E = S, Se, Te) nanotubes *via* ion exchange reaction at relatively low reaction temperatures.[159] These lead chalcogenide nanotubes, which self-organized from nanocrystals that displayed a quantum confinement effect as strong as that reported for quantum dots,[160,161] were presumed to be remarkably different from single-crystalline lead chalcogenide nanotubes. Although these nanotubes might not yet be readily used for device applications, mainly due to their rough inner surface and polycrystalline nature, this work demonstrates the extended concept of applying the ion exchange reaction for the synthesis of one-dimensional hollow nanostructures.

5. Ion exchange synthesis of hollow polyhedron micro/nano structures

The equilibrium shape of a crystal is determined by the relative specific surface energies associated with its facets.[162–171] The Wulff facets theorem states that at equilibrium, a crystal is bounded by facets giving a minimum total surface energy.[172] Different from hollow spheres and tubular structures, which correspond to stable growth faces, hollow polyhedra always correspond to a growth direction perpendicular to the growth facet with a high energy and high-index.[173–175] It is thus somewhat difficult to synthesize shape-controlled nanocrystals that are enclosed by high-index facets because of their high surface energy.[176–179] This is due to the fact that crystal growth rates in the direction perpendicular to a high-index plane are usually much faster than those along the normal direction of a low-index plane, so high-index planes are observed to rapidly disappear during the formation of a polyhedron.

Usually, high-index planes have a greater density of unsaturated atomic steps, ledges, and kinks, which can serve as active sites for breaking chemical bonds.[180] For example, fundamental studies on the single-crystal surfaces of bulk Pt have shown that high-index planes exhibit much higher catalytic activity than common, stable, low-index planes, such as (111) and (100).[181]

5.1. Hollow octahedron micro/nano structures

In addition to the hollow spheres and tubes, the ion exchange reaction can also be applicable in creating hollow polyhedral nanostructures. The synthesis of a hollow octahedron was demonstrated in the recent synthesis of CdS octahedron through an ion exchange reaction between solid $CdMoO_4$ and Cd^{2+} solution.[182] The hollow CdS octahedron was easily formed when S^{2-} ions were added to the $CdMoO_4$ solution and hydrothermally treated at 120 °C for 24 h *via* the dissolution and ion exchange process. As shown in Fig. 15a, a large scale of CdS microcages with well-preserved octahedral morphology was synthesized. High-resolution images revealed that the obtained octahedra exhibit rather rough surfaces (Fig. 15b) in contrast to the smooth surface of the precursors and had an average size of about 600 nm, which was slightly larger than that of the $CdMoO_4$ precursor (*ca.* 500 nm).

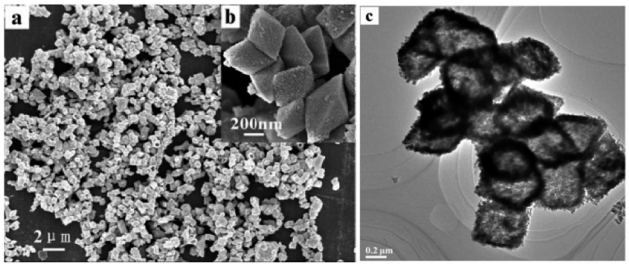

Fig. 15 (a and b) FESEM images and (c) TEM image of CdS microcages obtained through hydrothermal reaction with Na_2S as the sulfur source at 120 °C for 24 h. Reproduced with permission from ref. 182, copyright 2007 American Chemical Society.

Cd^{2+} dissolved from $CdMoO_4$ could rapidly react with S^{2-} to form an interconnected CdS shell around the external surface of the $CdMoO_4$ crystal, which was at the basis of the anion exchange reaction. Simultaneously, the S^{2-}/Cd^{2+} diffusion pair was also formed at the interface. After that, this growth process was followed by the formation of stable CdS phase surrounding the original $CdMoO_4$ crystals, leading to an outward diffusion of Cd cations and an inward flow of fast moving vacancies to the vicinity of the porous CdS shells. Finally, the hollow octahedral microcage with a hollow interior was formed and a relatively compact shell until the Cd^{2+} completely diffuses outward through the CdS shell and reacts with S^{2-}.

5.2. Hollow 18-facet polyhedron nanocrystals

It is more difficult to obtain 18-face polyhedron nanocrystals compared with the previously reported octahedron nanocrystals due to an increase in the high index faces. Recently, hollow 18-facet Cu_7S_4 polyhedron nanorods synthesized from a cubic Cu_2O nanoparticle precursor were reported by Qian and co-workers.[10] The reaction was performed in a highly pressurized autoclave through an ion exchange reaction coupled with a redox reaction.

The reported synthetic strategy involved the following processes: first, cubic Cu_2O nanoparticles were first prepared by adding a weak reductive agent (ascorbic acid solution) into Cu^{2+} aqueous solution with the use of PVP (poly(vinylpyrrolidone)) as a capping agent, hollow 18-facet Cu_7S_4 nanocages were obtained by adding a sulfur source (thiourea) under heating conditions. When thiourea was added and subjected to heat

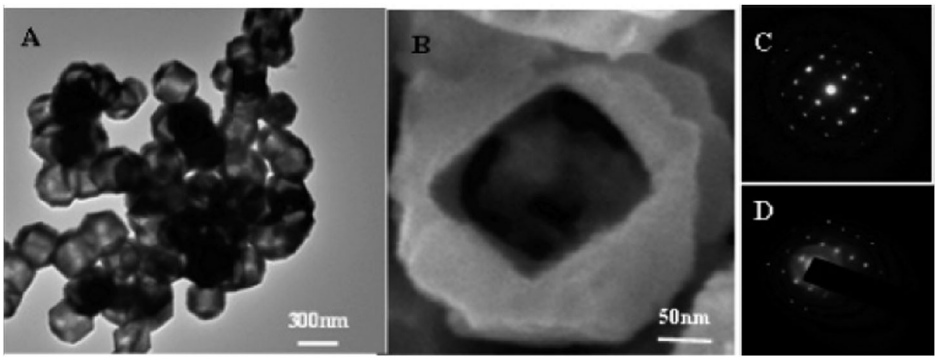

Fig. 16 (A) TEM of polyhedral Cu_7S_4 nanocrystals; (B) FESEM of broken polyhedral Cu_7S_4 with regular shape void; (C) and (D) SAED of two polyhedra with their square and hexagon facets oriented perpendicular to the electron beam. Reproduced with permission from ref. 10, copyright 2005 American Chemical Society.

treatment, sulfur ions were released from thiourea upon a hydrolyzation process. On the surface of the nanocubic Cu_2O, a thin layer of Cu_7S_4 was formed. This thin layer acts as an interface and separates the inner copper ions or Cu_2O from the outside sulfur ions. The formation of voids within the particle is due to a gradual outward movement of copper ions; as a result, particles tend to grow in size during the conversion processes. A TEM micrograph of the 18-facet Cu_7S_4 nanocrystals is displayed in Fig. 16A. The result in Fig. 16B shows the existence of voids within the nanocrystals. The authors also showed that the structure of Cu_7S_4 polyhedron facets was featured with single crystalline nanostructures by using SAED measurements (Fig. 16C and D).

6. Ion exchange synthesis of other complex nanostructures

Although the method of using ion exchange reaction to prepare hollow micro/nanostructure materials is quite straightforward and simple,[183–188] extensions of the method including partial ion exchange reactions can be used to produce very complicated nanostructures. For example, microrings and hemispheres can be produced *via* the addition of the local dissolution reaction and core–shell structures can be obtained by dual ion exchange reaction, as described below.

6.1. Microrings and hemisphere micro/nanostructures

Wang *et al.* were the first to study the freestanding single-crystal complete nanorings of zinc oxide induced by spontaneous self-coiling process during the growth of polar nanobelts in 2001.[189] They demonstrated that the nanoring was initiated by circular folding of a nanobelt, caused by long range electrostatic interactions. Coaxial and uniradial loop-by-loop winding of the nanobelt formed a complete ring. The self-coiling was thought to be driven by minimizing the energy contributed by polar charges, surface area and elastic deformation. Subsequently Shen and Chen proposed another synthetic approach for the first synthesis of $Ag_2V_4O_{11}$ nanorings and microloops formed by the self-coiling of $Ag_2V_4O_{11}$ nanobelts, which were resulted from a hydrothermal process.[190] The $Ag_2V_4O_{11}$ nanorings were formed by the self-coiling of one single-crystalline $Ag_2V_4O_{11}$ nanobelt, while the microloops were formed by several nanobelts. An ion exchange route to microrings and hemispheres was recently demonstrated.[191] Fig. 17 displays SEM micrographs of hollow ZnO microrings and hemispheres *via* the ion replacement reaction of $Zn_5(CO_3)_2(OH)_6$ microspheres and OH^- solution at room temperature. SEM imaging (Fig. 17A) reveals that hollow spheres are formed, while many of them have an open 'mouth' (Fig. 17B and C). In the samples, ZnO microrings can be identified, as shown in Fig. 17D. The wall of microrings consists of many nanocrystals, which are connected to each other to form a circularly shaped ring. Microring and hemisphere structures were prepared by an exchange reaction between $Zn_5(CO_3)_2(OH)_6$ and OH^- by the following reactions:

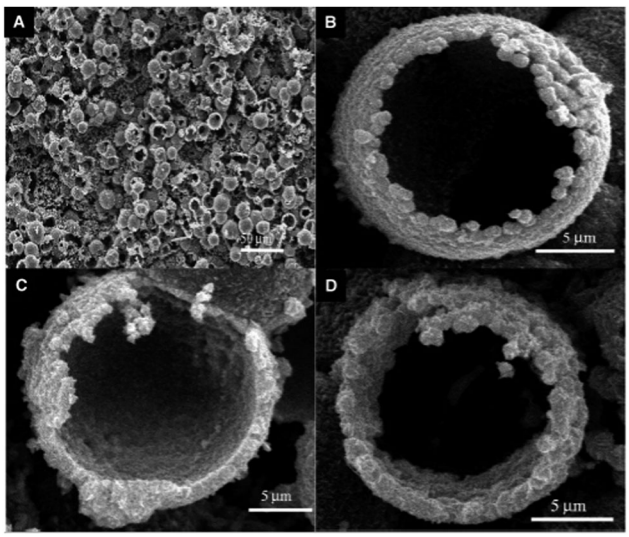

Fig. 17 SEM images of hollow ZnO architectures by employing $Zn_5(CO_3)_2(OH)_6$ microspheres as the sacrificial template. (A) Overall product morphology. (B) Hollow ZnO architecture composed of nanocrystals. (C) Hemispherical ZnO architecture. (D) Circular shaped ZnO architecture. Reproduced with permission from ref. 191, copyright 2006 American Chemical Society.

$$Zn_5(CO_3)_2(OH)_6(s) \rightarrow Zn^{2+} + OH^- + CO_3^{2-} \quad (3)$$

$$Zn^{2+} + OH^- \rightarrow ZnO(s) + H_2O \quad (4)$$

$$ZnO + OH^- \rightarrow Zn(OH)_4^{2-} \quad (5)$$

A possible formation mechanism for the hollow ZnO microrings was also proposed. Initially, ZnO microspheres can be formed *in situ via* a reaction between $Zn_5(CO_3)_2(OH)_6$ microsphere templates and KOH solution. Driven by the alkali solution, OH^- in solution diffuses into the $Zn_5(CO_3)_2(OH)_6$ microsphere surface. Simultaneously, $Zn_5(CO_3)_2(OH)_6$ microspheres dissociate to produce Zn^{2+}, which diffuses outward. Hollow ZnO microspheres were then immediately formed due to a driving force caused by the Kirkendall diffusion difference[37] associated with Zn^{2+} and OH^- in solution. ZnO spheres can be dissolved by KOH solution since ZnO has an amphoteric character. An excess of OH^- anion results in complete conversion of the already formed $Zn_5(CO_3)_2(OH)_6$ sphere into microrings or hemispheres by selectively dissolving the core and their surface. At low OH^- anion concentrations, the resulting ion exchange reaction produces completely hollow microspheres. The general challenges in the synthesis of microring structures lie in the improvement of the yield of the microrings. This work demonstrates that in addition to nanoscale fabrication of hollow crystals, the Kirkendall-type mass transport,[193–201] when coupled with interfacial chemical reactions, can be a powerful approach for both organization of individual nanoscale building blocks and the generation of interior spaces within organized structures.[192]

6.2. Core–shell micro/nanostructures

Core–shell structured materials often exhibit improved physical and chemical properties over their single-component counterparts and hence are potentially useful for a broader range of applications.[202–208] Therefore, methods to synthesize such materials with controlled precision have long been sought.[209–214] Although a variety of procedures have already been employed, several difficulties have limited the application of the final materials.[215] Moreover, even though the advantages of uniformly coated and stable colloidal particles have been recognized for years, the synthesis of core–shell structures has remained a technical challenge.

To obtain core–shell structured ZnO–ZnS, the dual ion exchange reaction among $Zn_5(CO_3)_2(OH)_6$ microspheres, OH^-, and S^{2-} in Na_2S solution at room temperature was recently employed.[139] Fig. 18 shows representative SEM images of core–shell nanostructured ZnO–ZnS composites formed by the ion replacement reaction between $Zn_5(CO_3)_2(OH)_6$ microspheres and Na_2S in solution at room temperature. The samples (Fig. 18) retain their spherical morphology within the core–shell structures. Fig. 18B shows a high-magnification SEM image of broken microspheres, from which the inner core can be seen, clearly displaying core–shell structures. A careful observation of Fig. 18C shows that the inner core was composed of many nanoparticles, and the core–shell structured ZnO–ZnS spheres had an average size of 10 μm. EDX spectroscopy was used to determine its chemical composition (Fig. 18D), which exhibited the presence of Zn, O and S elements.

The formation of core–shell ZnO–ZnS structures based on $Zn_5(CO_3)_2(OH)_6$ microspheres precursors appeared to be different

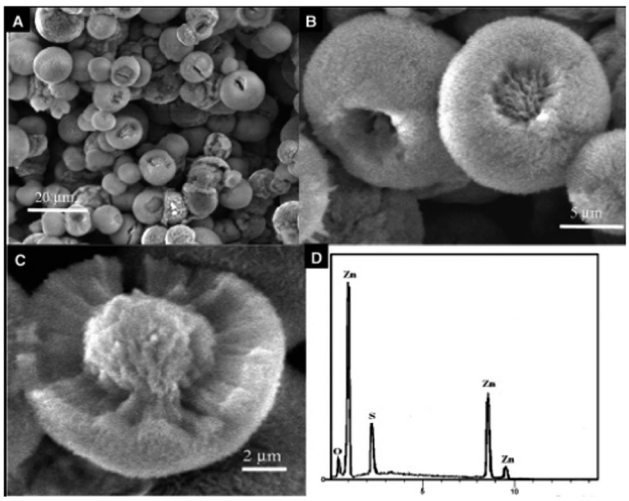

Fig. 18 Core–shell structured ZnO–ZnS composites by the ion replacement reaction of $Zn_5(CO_3)_2(OH)_6$ microspheres and Na_2S in solution at room temperature. (A) Overall product morphology. (B) Typical broken core–shell structures. (C) A core–shell structure with the broken core and shell. (D) EDX spectrum from the surface of core–shell structures. Reproduced with permission from ref. 191, copyright 2006 American Chemical Society.

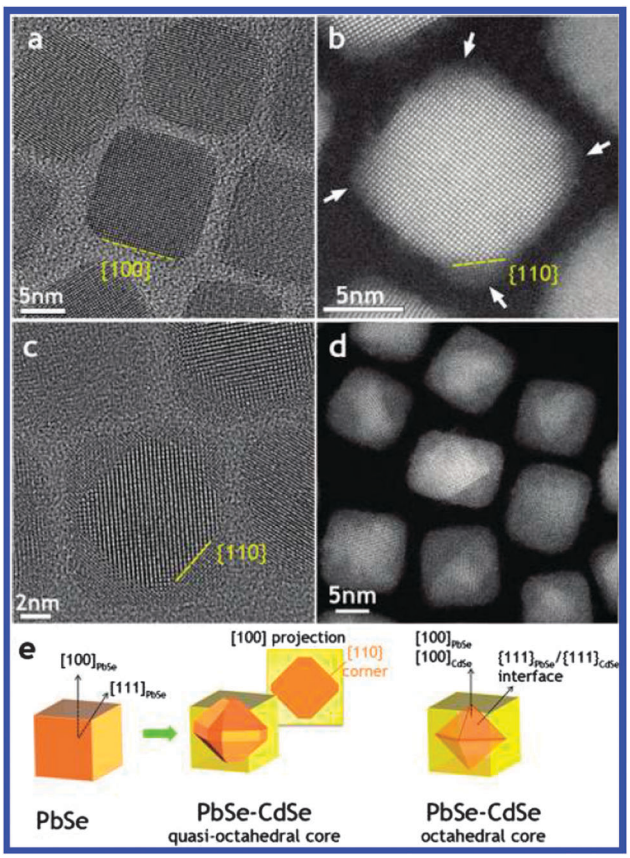

Fig. 19 (a) HR-TEM image of cube-shaped PbSe nanocrystals; (b and d) HAADF-STEM and (c) HRTEM images of PbSe/CdSe nanocrystals; (e) sketch of the structural transformation from pure PbSe cube-shaped NCs (left) to core–shell PbSe/CdSe nanocrystals. Reproduced with permission from ref. 218, copyright 2012 American Chemical Society.

compared with that of previous reports on ZnO hollow spheres, in which the formation of an empty structure was attributed to the fundamental solid-state phenomenon,[64] dealing with the movement of the interface between a diffusion couple. The conversion from $Zn_5(CO_3)_2(OH)_6$ microspheres to core–shell structured ZnO–ZnS composites was attributed to the difference of the solubility product for $ZnCO_3$ (1.2×10^{-10}), ZnO and ZnS (1.2×10^{-24}) at the same temperature. Compared with $ZnCO_3$, ZnO and ZnS are more thermodynamically stable due to their lower solubility products.

Recently, it has been shown that colloidal PbSe–CdSe core–shell nanostructures can be easily synthesized starting from nearly spherical PbSe cores using a Cd^{2+} for Pb^{2+} cationic exchange process.[216,217] Later, Casavola *et al.* demonstrated that PbSe–CdSe core–shell nanocrystals of different geometries can be obtained using PbSe nanocrystals as starting materials through an anisotropic cation exchange reaction.[218] Fig. 19 displays an overview of cubic PbSe NCs before (Fig. 19a) and after an ion exchange reaction (Fig. 19b–d). It is clearly shown that the nanocrystals can effectively preserve their size and shape, whereas the formation of crystalline CdSe is confirmed by EDX and high angle annular dark field (HAADF) scanning transmission electron microscopy (STEM) analyses. Control experiments showed no significant change in particle structure and properties over time when the temperature was kept constant throughout the synthesis. In principle, the ion exchange reaction can be employed as a general method for the synthesis of core–shell nanomaterials.

7. Potential applications of hollow structured materials

Hollow materials exhibit multiple interesting physical properties such as low density, high surface-to-volume ratio and low coefficients of thermal expansion than comparable solid nanostructures. The breakthrough of ion exchange synthetic methodologies for the synthesis of hollow structures has provided opportunities for their application in energy, electronics, sensing, mechanics, optics and other sectors. Their unique structure can also provide reduced lengths for both mass and charge transport. Due to these advantages, a significant volume of research has been carried out on the application of hollow structured materials ranging from lithium-ion batteries, photocatalysis, wastewater treatment and sensing.[219–221] Hereafter we will discuss notable examples of recent progress in developing applications.

Lithium-ion batteries have been considered the most important energy storage devices for hybrid, plug-in hybrid, electric vehicle applications, power backup and portable power tools. In terms of performance limitations, the volume change induced by mechanical strain generated during cycling is considered to be the main reason for capacity fading and poor cycling life.[220,221] An effective strategy to overcome this challenge is to fabricate hollow nanostructured electrode materials as they can provide large surface area for more lithium storage sites as well as reduced transport lengths for Li^+ ion diffusion and electron transport. On the other hand, the hollow interior provides extra free space for alleviating the structural strain and accommodating the large volume changes during repeatable cycling. For example, various hollow structures of metal oxides[17,93,222–225] have been successfully designed for promising high-energy electrode materials. Lou *et al.*[222] demonstrate a general ion exchange method toward the large-scale synthesis of complex hollow microboxes between a unique metal–organic frameworks (MOFs) template and different substances. Such hollow structures could provide high gravimetric energy densities and higher volumetric energy densities than their solid counterparts. The ion exchange reaction between the solid PB microcubes and liquid alkaline solution produces $Fe(OH)_3$ hollow structures, which could be easily converted to α-Fe_2O_3

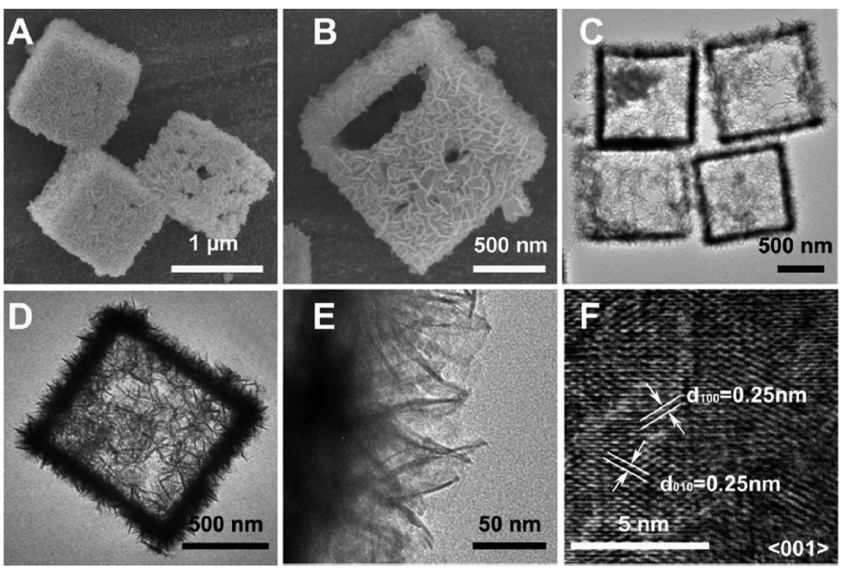

Fig. 20 FESEM (A and B) and TEM (C–F) images of hierarchically single-shelled Fe_2O_3 microboxes obtained by the reaction of $Fe_4[Fe(CN)_6]_3$ cubes with 0.2 M NaOH under hydrothermal conditions. Reproduced with permission from ref. 222, copyright 2013 American Chemical Society.

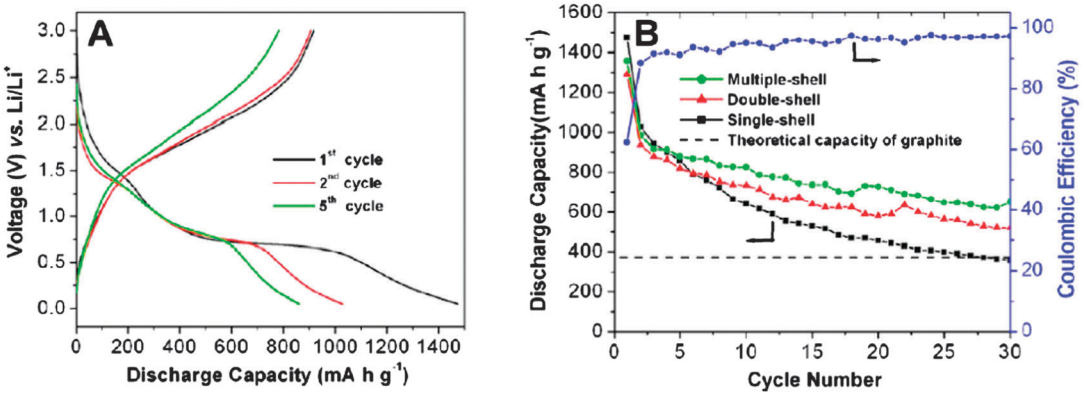

Fig. 21 (A) Discharge–charge voltage profiles of single-shelled Fe_2O_3 microboxes. (B) Cycling performance of single shelled, double-shelled, and multiple-shelled Fe_2O_3 microboxes. Reproduced with permission from ref. 222, copyright 2013 American Chemical Society.

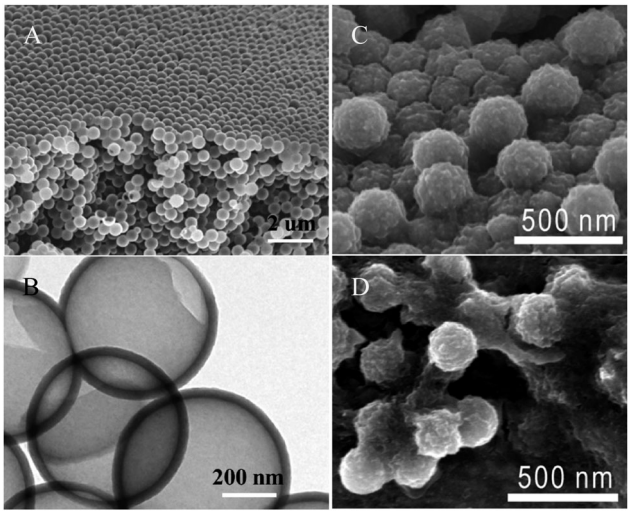

Fig. 22 Si hollow spheres: (A and B) before cycling, (C) after 40 cycles, and (D) after 700 cycles. Reproduced with permission from ref. 226, copyright 2011 American Chemical Society.

via a low temperature annealing process. From the SEM images, the hollow structures are well maintained (Fig. 20A and B). As displayed in TEM images (Fig. 20C–F), it shows a crystalline character with a well resolved lattice spacing. With this ion exchange method, single-shelled, double-shelled and multiple-shelled Fe_2O_3 microboxes were prepared, and the multiple-shelled Fe_2O_3 microboxes exhibit higher specific capacity than those of single-shelled and double-shelled Fe_2O_3 microboxes (Fig. 21). The large void space of these structures may enhance their capacity of retention by reversibly accommodating large volume changes and may provide extra space for the storage of lithium ions, which in turn is beneficial for enhancing the specific capacity of the batteries. However, certain features of hollow structure materials may also cause performance issues. For example, high electrolyte/electrode surface area may lead to more significant side reactions.

To understand the cycling performance, Cui *et al.*[226] examine the morphology evolution of the hollow nanospheres before and after lithiation. Before lithiation the microspheres show a smooth surface (Fig. 22A and B). After several cycles the surface

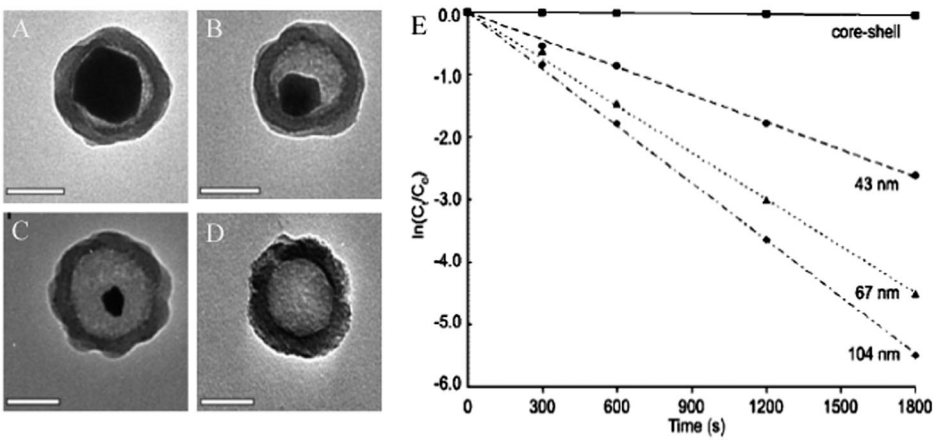

Fig. 23 (A–D) Transmission electron microscopy images of Au@SiO_2 hollow nanoreactor frameworks with different sizes. The scale bars represent 100 nm. (E) Plot of $\ln(C_t/C_0)$ *versus* time for each nanoreactor framework, where C_t and C_0 are *p*-nitrophenol concentrations at time *t* and 0, respectively. Reproduced with permission from ref. 228, copyright 2008 Wiley-VCH Verlag GmbH & Co. KGaA.

of the microtubes becomes rough and the hollow structure is conspicuously maintained, although there exists a change in the size, perhaps due to solid electrolyte interphase (SEI) formation and the volume change of the hollow nanospheres (Fig. 22C and D). Hollow structures show better capacity retention due to the maximization of the beneficial effects arising from the hollow and hierarchical structures, which could significantly reduced diffusion-induced stress and better withstand the repeated volume expansion/contraction and facilitate the lithium ions insertion with reduced diffusion length.

In the field of photocatalysis, significant efforts have focused on developing photocatalysts with high activities. Due to their high surface to volume ratio, hollow micro/nanostructure materials can greatly improve photocatalytic activity and conversion efficiency. For example, Huang *et al.*[227] reported an anion exchange strategy to synthesize Bi_2WO_6 hollow microspheres, which show high CO_2 adsorption capacity and high visible light photocatalytic conversion efficiency of CO_2 into methanol. The enhanced visible light CO_2 photocatalytic conversion efficiency was attributed to the large surface area and high CO_2 adsorption capacity. Song *et al.* fabricated an ideal hollow nanoreactor system comprising gold cores with empty inner space. The hollow particles exhibited a size-dependent catalytic activity for *p*-nitrophenol (Fig. 23),[228] thus demonstrating a promising platform to study various heterogeneous catalytic reactions. More recently, Ye *et al.*[229] fabricated hollow Ag_2ZnGeO_4 spheres by ion exchange reaction between Zn_2GeO_4 and Ag^+ ions. As shown in Fig. 24, the product is composed of uniform spherical particles with hollow structures. The chemical composition of the as-prepared hollow Ag_2ZnGeO_4 spheres was investigated by EDX Mapping (element distribution images), indicating that Ag, Zn, Ge and O are uniformly distributed (Fig. 24d). The formation of hollow spheres can be attributed to an Ostwald ripening process, involving the dissolution of smaller crystals and re-growth on larger crystals during aging. The authors also investigated photocatalytic activity by degradation of rhodamine B dye (RhB) under visible light. Fig. 25 displays the experimental results of RhB photodegradation over Ag_2ZnGeO_4 hollow spheres and bulk Ag_2ZnGeO_4 (as reference sample) under visible light irradiation. The fractional rate over hierarchical Ag_2ZnGeO_4 hollow spheres was found to be about 2.5 times as high as that over reference bulk Ag_2ZnGeO_4. The observed high activities are attributed to the high surface/volume ratios of the materials, compared to dense spheres of similar size, because their open hollow structure enables both the outer and inner surfaces of the catalyst to come into contact with the reactants, thus enhancing the catalytic process. Therefore, exploitation of hollow structure photocatalysts that display high activity is crucial for photocatalytic conversion to high-energy-content fuels.

Hollow Au nanomaterials can be used as imaging and diagnostics agents in biomedicine, since hollow Au nanostructures can be tuned to strongly absorb in the near-infrared (NIR) region where optical transmission through tissue is optimal.[230]

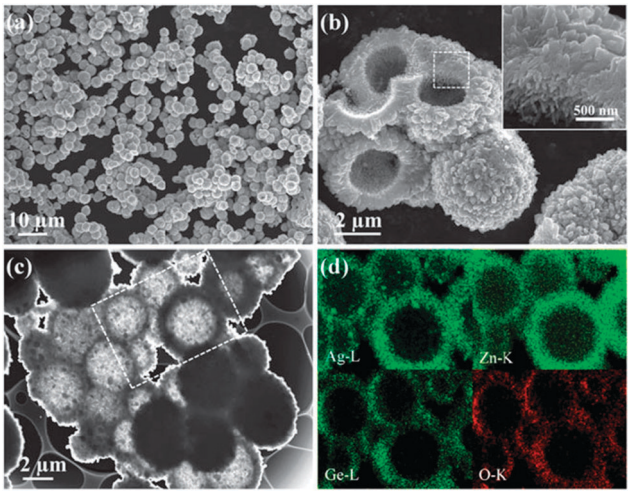

Fig. 24 (a and b) SEM images (inset of (b) is the magnified SEM image taken from the marked square area); (c) STEM image of Ag_2ZnGeO_4 prepared using $AgNO_3$ for 12 h; (d) STEM elemental mapping of Ag, Zn, Ge, and O taken from the square area marked in (c). Reproduced from ref. 229 with permission from the Centre National de la Recherche Scientifique (CNRS) and The Royal Society of Chemistry.

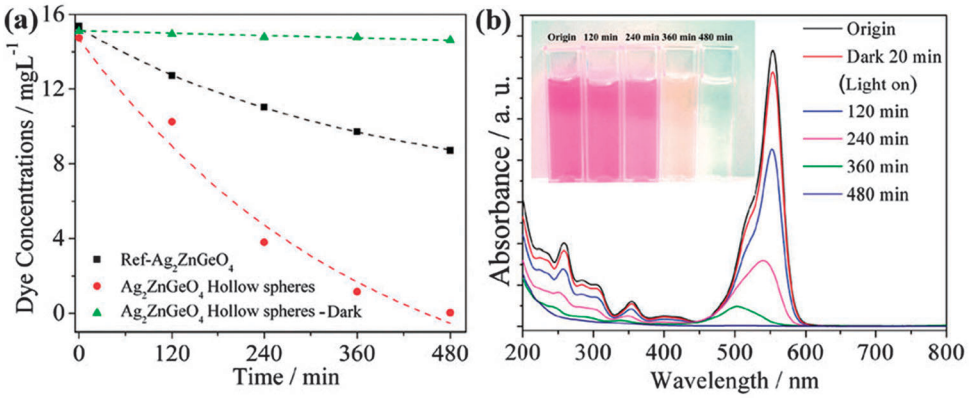

Fig. 25 (a) RhB degradation over the as prepared hierarchical Ag_2ZnGeO_4 hollow spheres and reference sample Ag_2ZnGeO_4 under visible light; (b) UV-vis spectral changes of RhB aqueous solution. Reproduced from ref. 229 with permission from the Centre National de la Recherche Scientifique (CNRS) and The Royal Society of Chemistry.

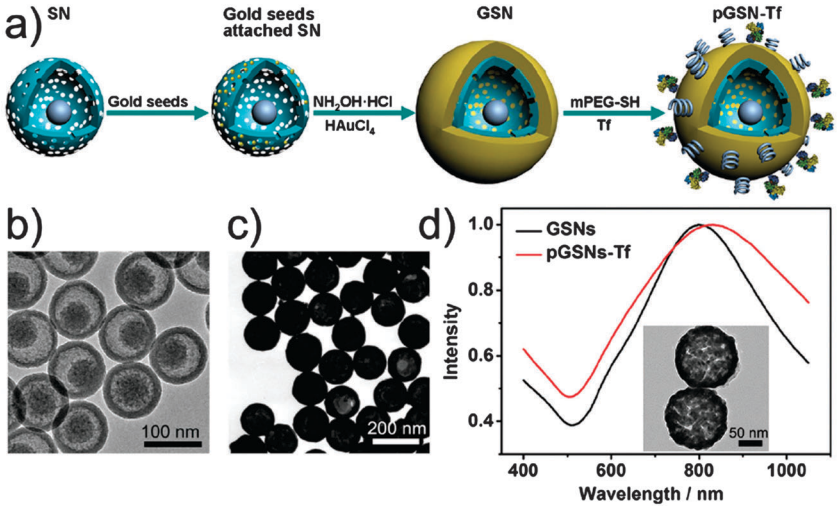

Fig. 26 (a) Schematic diagram of gold nanoshells on silica nanorattles (GSNs) synthesis and bioconjugation. (b) TEM image of silica nanorattles (SNs). (c) TEM image of GSNs. (d) Extinction spectra of pGSNs and Tf and PEG (polyethylene glycol) functionalized gold nanoshells on silica nanorattles (pGSNs-Tf), the inset is the TEM image of pGSNs-Tf. Reproduced with permission from ref. 230, copyright 2012 Wiley-VCH Verlag GmbH & Co. KGaA.

The gold nanoshells on silica nanorattles (GSNs) synthesis and bioconjugation is schematically shown in Fig. 26a. The structures consist of a thin gold nanoshell and a monodispersed mesoporous silica nanorattles (SN) core, conferring many advantages. SNs with a size of 101 nm and GSNs with compact gold shells of $\sim$30 nm were obtained (Fig. 26b and c). The GSNs have tunable optical property as NIR light absorbing agents and high payload, sustained drug release as drug delivery system. The authors observed the broadening and red-shifted of the extinction spectra for pGSNs-Tf due to the higher refractive index of PEG and Tf layer with respective to H_2O (Fig. 26d). By targeting cancer cells with these hollow particles and irradiating with infrared light, a local irreversible ablation can be generated, with a therapeutic effect on targeted cancer cells. Such photothermal therapy is less invasive than chemotherapy or surgery and holds strong promise as a new form of cancer treatment where the hollow structure plays an important role in improving performance.

8. Conclusions and perspectives

Each synthesis approach of hollow materials has specific merits and inevitable weaknesses. The ion exchange synthesis provides a simple and versatile route to fabricate hollow micro/nanostructure materials with uniform size but a number of different compositions with respect to their precursors.

This review provides an overview of a variety of ion exchange reaction processes that have been developed to generate hollow structures. We broadly divided these hollow structures into three categories, by sorting them on the basis of the shape of the product: (I) ion exchange synthesis for hollow micro/nanospheres; (II) ion exchange synthesis of hollow micro/nanotubes; (III) ion exchange synthesis of hollow polyhedral micro/nanostructures. We also briefly discuss a number of other attractive structures such as core–shell structures prepared *via* dual ion exchange reaction. Recent work showed that it is feasible to further increase the diversity of ion exchange synthesis that can be used in the ion exchange of pre-synthesized nanomaterials to produce multifunctional hollow and core–shell spheres with a variety of properties.

The ion exchange reaction can be effectively used for the synthesis of hollow micro/nanostructure materials from insoluble solids. An overall extraction of species close to 100% can be achieved if ion exchange between cations or anions were 100% efficient, even if the species has very low solubility products and solution concentrations. The solubility product of the species must be large enough to result in at least traces of the ion species in solution for the process of enhanced dissolution extraction to succeed. There is no topotactic relationship between the crystal structures of the precursor and the resulting hollow structures as there is a large change in the volume or lattice parameters during ion exchange process; as a consequence, preserving the crystal structure feature during the ion exchange reaction is a major challenge. Many factors related to the reaction should be taken into consideration and systematically examined: for example, the reaction mechanism; the rate of transformation; the volume change involved in the reaction; and the growth direction of the resultant lattice. In some cases, the diameter and shape of the precursor might also play a vital role in determining the volume change, growth direction and thus structure evolution of the product. In addition, a comprehensive and in depth understanding of the relationship between the structures and functionalities of the hollow structures has not yet been reported. Therefore, it is urgent to establish theoretical models to direct a more rational design towards the synthesis of future functional materials.

There has also been rapid growth in the development of hollow structures for potential applications. Hollow structures represent a new class of interesting and important micro/nanostructures because of their superior performance in areas

such as energy storage, photocatalysis, energy conversion, electronics, optoelectronics and sensing. The most promising developments may lie in the future as newer materials with hollow structures synthesized by ion exchange reaction continue to be developed. All these aspects will become interesting and exciting subjects for fundamental and applied studies in physics, chemistry and materials science and engineering. There are almost unlimited research opportunities that are being pursued by many laboratories around the world in this general area of hollow structures. The scientific and technical potential of these nanostructures are enormous and the future of this sub-field of nanoscience is promising and exciting. However, the development of large-scale and low-cost synthesis of these hollow materials in a non-agglomerated state and with uniform shape is still required before they can find widespread use in multiple applications.

Acknowledgements

F.R. acknowledges funding from NSERC (Discovery Grant, Strategic Project Grant and CRD project in collaboration with Plasmionique, Inc.), from FQRNT and MDEIE and is grateful to the Canada Research Chairs program for partial salary support. F.R. is also grateful to the Alexander von Humboldt Foundation for a F.W. Bessel Award (2011).

References

1 F. Rosei, *J. Phys.: Condens. Matter*, 2004, **16**, S1373.
2 F. Patolsky, B. P. Timko, G. H. Yu, Y. Fang, A. B. Greytak, G. Zheng and C. M. Lieber, *Science*, 2006, **313**, 1100.
3 C. Yan, A. Dadvand, F. Rosei and D. F. Perepichka, *J. Am. Chem. Soc.*, 2010, **132**, 8868.
4 C. Yan, J. Liu, F. Liu, J. Wu, K. Gao and D. Xue, *Nanoscale Res. Lett.*, 2008, **3**, 473.
5 F. Variola, J. Yi, L. Richert, J. D. Wuest, F. Rosei and A. Nanci, *Biomaterials*, 2008, **29**, 1285.
6 L. Richert, F. Vetrone, J. Yi, S. F. Zalzal, J. D. Wuest, F. Rosei and A. Nanci, *Adv. Mater.*, 2008, **20**, 1448.
7 F. Vetrone, F. Variola, P. Tambasco, D. Oliveira, S. F. Zalzal, J. Yi, J. Sam, K. F. Bombonato-Prado, A. Sarkissian, D. F. Perepichka, J. D. Wuest, F. Rosei and A. Nanci, *Nano lett.*, 2009, **9**, 659.
8 C. Yan and D. Xue, *Adv. Mater.*, 2008, **20**, 1055.
9 C. Yan, L. Nikolova, A. Dadvand, C. Harnagea, A. Sarkissian, D. F. Perepichka and D. Xue, *Adv. Mater.*, 2010, **22**, 1741.
10 (*a*) H. Cao, X. Qian, C. Wang, X. Ma, J. Yin and Z. Zhu, *J. Am. Chem. Soc.*, 2005, **127**, 16024; (*b*) F. Bai, Z. Sun, H. Wu, R. Haddad, X. Xiao and H. Fan, *Nano Lett.*, 2011, **11**, 3759.
11 (*a*) A. Khanal, Y. Inoue, M. Yada and K. Nakashima, *J. Am. Chem. Soc.*, 2007, **129**, 1534; (*b*) J.-H. Lee, Y.-M. Huh, Y. Jun, J. Seo, J. Jang, H.-T. Song, S. Kim, E.-J. Cho, H.-G. Yoon, J.-S. Suh and J. Cheon, *Nat. Med.*, 2007, **13**, 95.
12 M. E. Medina, A. E. Platero-Prats, N. Snejko, A. Rojas, A. Monge, F. Gandara, E. Gutierrez-Puebla and M. A. Camblor, *Adv. Mater.*, 2011, **23**, 5283.
13 S. Peng and S. H. Sun, *Angew. Chem., Int. Ed.*, 2007, **46**, 4155.
14 B. Wang, J. S. Chen, H. B. Wu, Z. Y. Wang and X. W. Lou, *J. Am. Chem. Soc.*, 2011, **133**, 17146.
15 X. Lou, L. Archer and Z. Yang, *Adv. Mater.*, 2008, **20**, 3987.
16 L. Zhou, D. Y. Zhao and X. W. Lou, *Angew. Chem., Int. Ed.*, 2012, **51**, 239.
17 X. Lai, J. E. Halperta and D. Wang, *Energy Environ. Sci.*, 2012, **5**, 5604.
18 Y. Zhao and L. Jiang, *Adv. Mater.*, 2009, **21**, 3621.
19 J. Liu, F. Liu, K. Gao, J. Wu and D. Xue, *J. Mater. Chem.*, 2009, **19**, 6073.
20 Q. F. Zhang, T. R. Chou, B. Russo, S. A. Jenekhe and G. Z. Cao, *Angew. Chem., Int. Ed.*, 2008, **47**, 2402.
21 H. J. Fan, M. Knez, R. Scholz, D. Hesse, K. Nielsch, M. Zacharias and U. Gosele, *Nano Lett.*, 2007, **7**, 993.
22 B. Liu and H. C. Zeng, *Chem. Mater.*, 2007, **19**, 5824.
23 H. G. Yang and H. C. Zeng, *J. Phys. Chem. B*, 2004, **108**, 3492.
24 Y. Chang, J. J. Teo and H. C. Zeng, *Langmuir*, 2005, **21**, 2005.
25 B. Liu and H. C. Zeng, *Small*, 2005, **1**, 566.
26 B. X. Li, G. X. Rong, Y. Xie, L. F. Huang and C. Q. Feng, *Inorg. Chem.*, 2006, **45**, 6404.
27 H. G. Yu, J. G. Yu, S. W. Liu and S. Mann, *Chem. Mater.*, 2007, **19**, 2007.
28 H. J. Liu, Y. H. Ni, M. Han, Q. Liu, Z. Xu, J. N. Hong and X. Ma, *Nanotechnology*, 2005, **16**, 2908.
29 H. L. Xu, W. Z. Wang, W. Zhu and L. Zhou, *Nanotechnology*, 2006, **17**, 3649.
30 Y. H. Zheng, Y. Cheng, Y. S. Wang, L. H. Zhou, F. Bao and C. Jia, *J. Phys. Chem. B*, 2006, **110**, 8284.
31 X. B. Cao, L. Gu, L. Zhuge, W. J. Gao, W. C. Wang and S. F. Wu, *Adv. Funct. Mater.*, 2006, **16**, 896.
32 F. Caruso, R. A. Caruso and H. Mohwald, *Science*, 1998, **282**, 1111.
33 V. Salgueirino-Maceira, M. Spasova and M. Farle, *Adv. Funct. Mater.*, 2005, **15**, 1036.
34 F. Caruso, M. Spasova, V. Saigueirino-Maceira and L. M. Liz-Marzan, *Adv. Mater.*, 2001, **13**, 1090.
35 H. Shiho and N. Kawahashi, *Colloid Polym. Sci.*, 2000, **278**, 270.
36 N. Kawahashi, C. Persson and E. Matijevic, *J. Mater. Chem.*, 1991, **1**, 577.
37 Y. D. Xia and R. Mokaya, *J. Mater. Chem.*, 2005, **15**, 3126.
38 H. T. Schmidt and A. E. Ostafin, *Adv. Mater.*, 2002, **14**, 532.
39 D. H. W. Hubert, M. Jung and A. L. German, *Adv. Mater.*, 2000, **12**, 1291.
40 H. P. Hentze, S. R. Raghavan, C. A. McKelvey and E. W. Kaler, *Langmuir*, 2003, **19**, 1069.
41 T. Hirai, S. Hariguchi, I. Komasawa and R. J. Davey, *Langmuir*, 1997, **13**, 6650.
42 M. M. Wu, G. G. Wang, H. F. Xu, J. B. Long, F. L. Y. Shek, S. M. F. Lo, I. D. Williams, S. H. Feng and R. R. Xu, *Langmuir*, 2003, **19**, 1362.

43 C. E. Fowler, D. Khushalani and S. Mann, *Chem. Commun.*, 2001, 2028.
44 C. E. Fowler, D. Khushalani and S. Mann, *J. Mater. Chem.*, 2001, **11**, 1968.
45 J. X. Huang, Y. Xie, B. Li, Y. Liu, Y. T. Qian and S. Y. Zhang, *Adv. Mater.*, 2000, **12**, 808.
46 F. L. Du, Z. Y. Guo and G. C. Li, *Mater. Lett.*, 2005, **59**, 2563.
47 S. Kobayashi, N. Hamasaki, M. Suzuki, M. Kimura, H. Shirai and K. Hanabusa, *J. Am. Chem. Soc.*, 2002, **124**, 6550.
48 C. G. Go, *Angew. Chem., Int. Ed.*, 1999, **38**, 3155.
49 Y. Sun and Y. Xia, *Science*, 2002, **298**, 2176.
50 Y. Sun, B. Mayers and Y. Xia, *Adv. Mater.*, 2003, **15**, 641.
51 T. Nakashima and N. Kimizuka, *J. Am. Chem. Soc.*, 2003, **125**, 6386.
52 C. W. Guo, Y. Cao, S. H. Xie, W. L. Dai and K. N. Fan, *Chem. Commun.*, 2003, 700.
53 A. D. Dinsmore, M. F. Hsu, M. G. Nikolaides, M. Marquez, A. R. Bausch and D. A. Weitz, *Science*, 2002, **298**, 1006.
54 R. A. Caruso, J. H. Schattka and A. Greiner, *Adv. Mater.*, 2001, **13**, 1577.
55 Z. Yang, Z. Niu, Y. Lu, Z. Hu and C. C. Han, *Angew. Chem., Int. Ed.*, 2003, **42**, 1943.
56 J. J. Zhu, S. Xu, H. Wang, J. M. Zhu and H. Y. Chen, *Adv. Mater.*, 2003, **15**, 156.
57 Q. Peng, Y. Dong and Y. Li, *Angew. Chem., Int. Ed.*, 2003, **42**, 3027.
58 S. Iijima, *Nature*, 1991, **354**, 56.
59 J. Prashant, A. Lilac, A. Shaul and A. P. Alivisatos, *J. Am. Chem. Soc.*, 2010, **132**, 9997.
60 C. Yan and D. Xue, *J. Phys. Chem. B*, 2006, **110**, 1581.
61 C. Yan and D. Xue, *J. Phys. Chem. B*, 2006, **110**, 25850.
62 C. Yan and D. Xue, *J. Phys. Chem. B*, 2006, **110**, 11076.
63 K. P. Jain, L. Amirav, S. Aloni and A. P. Alivisatos, *J. Am. Chem. Soc.*, 2010, **132**, 9997.
64 Y. Yin, R. Rioux, C. Erdonmez, S. Hughes, G. Somorjai and A. Alivisatos, *Science*, 2004, **304**, 711.
65 P. de Viliers, J. Van Deventer and L. Lorenzen, *Miner. Eng.*, 1995, **8**, 1309.
66 F. Helfferich, *Ion Exchange*, McGraw-Hill Book Company, Inc., USA, 1962, pp. 226–245.
67 R. Kunin, in *Ion Exchange Resins*, ed. E. Robert, Kriegler Publishing Company, Huntington, New York, 1972.
68 D. H. Son, S. M. Hughes, Y. Yin and A. P. Alivisatos, *Science*, 2004, **306**, 1009.
69 L. Dlozik and R. Konenkamp, *Nano Lett.*, 2003, **3**, 651.
70 J. Krustok, J. Madasson, M. Altosaar and P. E. Kukk, *J. Phys. Chem. Solids*, 1990, **51**, 1013.
71 C. D. Lokhande, V. V. Bhad and S. S. Dhumure, *J. Phys.*, 1992, **25**, 315.
72 C. D. Lokhande and K. M. Gadave, *Mater. Chem. Phys.*, 1993, **36**, 119.
73 M. Ristova and M. Ristov, *Appl. Surf. Sci.*, 2001, **181**, 68.
74 L. Dloczik, R. Engelhardt, K. Ernst, S. Fiechter, I. Sieber and R. Konenkamp, *Appl. Phys. Lett.*, 2001, **78**, 3687.
75 X. Wang, P. Gao, J. Li, C. Summers and Z. Wang, *Adv. Mater.*, 2002, **14**, 1732.
76 Q. Wang, J. Li, G. Li, X. Cao, K. Wang and J. Chen, *J. Cryst. Growth*, 2007, **299**, 386.
77 E. J. Silvester, F. Grieser, B. A. Sexton and T. W. Healy, *Langmuir*, 1991, **7**, 2917.
78 M. V. Artemyev, V. S. Gurin, K. V. Yumashev, P. V. Prokoshin and A. M. Maljarevich, *J. Appl. Phys.*, 1996, **80**, 7028.
79 L. Ye, C. Wu, W. Guo and Y. Xie, *Chem. Commun.*, 2006, 4738.
80 L. Ye, W. Guo, Y. Yang, Y. Du and Y. Xie, *Chem. Mater.*, 2007, **19**, 6331.
81 T. Wu, H. Mayaffre, S. Kramer, M. Horvatic, C. Berthier, W. N. Hardy, R. X. Liang, D. A. Bonn and M. H. Julien, *Nature*, 2011, **477**, 7363.
82 O. E. Semonin, J. M. Luther, S. Choi, H. Y. Chen, J. B. Gao, A. J. Nozik and M. C. Beard, *Science*, 2011, **334**, 1530.
83 R. Das, P. Pachfule, R. Banerjee and P. Poddar, *Nanoscale*, 2012, **4**, 591.
84 S. B. Ogale, *Adv. Mater.*, 2010, **22**, 3125.
85 Z. P. Li, Q. Q. Zhao, W. L. Fan and J. H. Zhan, *Nanoscale*, 2011, **3**, 1646.
86 S. Agarwala, Z. H. Lim, E. Nicholson and G. W. Ho, *Nanoscale*, 2012, **4**, 194.
87 L. Vayssieres, *Adv. Mater.*, 2003, **15**, 464.
88 P. Atanasova, D. Rothenstein, J. J. Schneider, R. C. Hoffmann, S. Dilfer, S. Eiben, C. Wege, H. Jeske and J. Bill, *Adv. Mater.*, 2011, **23**, 4918.
89 P. X. Gao, Y. Ding, W. Mai, W. L. Hughes, C. Lao and Z. L. Wang, *Science*, 2005, **309**, 1700.
90 A. Chanaewa, B. H. Juarez, H. Weller and C. Klinke, *Nanoscale*, 2012, **4**, 251.
91 H. Kou, J. Wang, Y. Pan and J. Guo, *Mater. Chem. Phys.*, 2006, **99**, 325.
92 J. Liu and D. Xue, *Adv. Mater.*, 2008, **20**, 2622.
93 J. Liu and D. Xue, *Nanoscale Res. Lett.*, 2010, **5**, 1525.
94 C. B. Murray, C. R. Kagan and M. G. Bawendi, *Annu. Rev. Mater. Sci.*, 2000, **30**, 545.
95 Y. Huang, X. F. Duan, Y. Cui, L. J. Lauhon, K. H. Kim and C. M. Lieber, *Science*, 2001, **294**, 1313.
96 R. Viswanatha, D. M. Battaglia, M. E. Curtis, T. D. Mishima, M. B. Johnson and X. G. Peng, *Nano Res.*, 2008, **1**, 138.
97 Y. Cui and C. M. Lieber, *Science*, 2001, **291**, 851.
98 W. U. Huynh, J. J. Dittmer and A. P. Alivisatos, *Science*, 2002, **295**, 2425.
99 N. Tessler, V. Medvedev, M. Kazes, S. H. Kan and U. Banin, *Science*, 2002, **295**, 1506.
100 H. Li, M. Zanella, A. Genovese, M. Povia, A. Falqui, C. Giannini and L. Manna, *Nano Lett.*, 2011, **11**, 4964.
101 X. Gao, Y. Cui, R. M. Levenson, L. W. K. Chung and S. Nie, *Nat. Biotechnol.*, 2004, **22**, 969.
102 E. Groeneveld, S. Berkum, M. M. Schooneveld, A. Gloter, J. D. Meeldijk, D. Heuvel, H. C. Gerritsen and C. Donega, *Nano Lett.*, 2012, **12**, 749.

103 M. S. Wang, I. Kaplan-Ashiri, X. L. Wei, R. Rosentsveig, H. D. Wagner, R. Tenne and L. M. Peng, *Nano Res.*, 2008, **1**, 22.
104 A. Henglein, *Chem. Rev.*, 1989, **89**, 1861.
105 S. T. Lakshmikvmar, *Sol. Energy Mater. Sol. Cells*, 1994, **32**, 7.
106 B. Yuan, W. Luan and S. Tu, *CrystEngComm*, 2012, **14**, 2145.
107 A. A. Korzhuev, *Fiz. Khim. Obrab. Mater.*, 1991, **3**, 131.
108 Y. Wang and N. Herron, *J. Phys. Chem.*, 1991, **95**, 525.
109 T. C. Harman, P. J. Taylor, M. P. Walsh and B. E. La Forge, *Science*, 2002, **297**, 2229.
110 S. Sheldrick and M. Wachhold, *Angew. Chem., Int. Ed. Engl.*, 1997, **39**, 206.
111 G. Parkin, *Prog. Inorg. Chem.*, 1998, **47**, 1.
112 M. L. Steigerwald and L. E. Brus, *Acc. Chem. Res.*, 1990, **23**, 183.
113 G. D. Moona, S. Koa, Y. Mina, J. Zeng, Y. Xia and U. Jeonga, *Nano Today*, 2011, **6**, 186.
114 G. Zhang, W. Wang, Q. Yu and X. Li, *Chem. Mater.*, 2009, **21**, 969.
115 W. Zhu, W. Z. Wang and J. L. Shi, *J. Phys. Chem. B*, 2006, **110**, 9785.
116 P. H. C. Camargo, Y. H. Lee, U. Jeong, Z. Zou and Y. Xia, *Langmuir*, 2007, **23**, 2985.
117 Q. Peng, Z. Zhuang, X. Wang and Y. Li, *Small*, 2005, **1**, 216.
118 P. Camargo, Y. Lee, U. Jeong, Z. Zou and Y. Xia, *Langmuir*, 2007, **23**, 2985.
119 Y. Xiong, B. Mayers and Y. Xia, *Chem. Commun.*, 2005, 5013.
120 S. Z. Chu, S. Inoue, K. Wada, D. Li, H. Haneda and S. Awatsu, *J. Phys. Chem. B*, 2003, **107**, 6586.
121 C. T. Yip, H. T. Huang, L. M. Zhou, K. Y. Xie, Y. Wang, T. H. Feng, J. S. Li and W. Y. Tam, *Adv. Mater.*, 2011, **23**, 5624.
122 I. Avramov, *Nanoscale Res. Lett.*, 2007, **2**, 235.
123 O. K. Varghese, D. W. Gong, M. Paulose, K. G. One, E. C. Dickey and C. A. Grimes, *Adv. Mater.*, 2003, **15**, 624.
124 F. Meng and S. Jin, *Nano Lett.*, 2012, **12**, 234.
125 Y. Piao, J. Kim, H. B. Na, D. Kim, J. S. Baek, M. K. Ko, J. H. Lee, M. Shokouhimehr and T. Hyeon, *Nat. Mater.*, 2008, **7**, 242.
126 Y. R. Hacohen, E. Grunbaum, R. Tenne, J. Sloan and J. L. Hutchison, *Nature*, 1998, **395**, 336.
127 S. Uchida, R. Chiba, M. Tomiha, N. Masaki and M. Shirai, *Electrochemistry*, 2002, **70**, 418.
128 M. S. Sander, M. J. Cote, W. Gu, B. M. Kile and C. P. Tripp, *Adv. Mater.*, 2004, **16**, 2052.
129 L. Yadgarov, R. Rosentsveig, G. Leitus, A. Albu-Yaron, A. Moshkovith, V. Perfilyev, R. Vasic, A. I. Frenkel, A. N. Enyashin, G. Seifert, L. Rapoport and R. Tenne, *Angew. Chem., Int. Ed.*, 2012, **51**, 1148.
130 I. Wiese, R. Popovitz-Biro and R. Tenne, *Nanoscale*, 2013, **5**, 1499.
131 G. Radovsky, R. Popovitz-Biro, M. Staiger, K. Gartsman, C. Thomsen, T. Lorenz, G. Seifert and R. Tenne, *Angew. Chem., Int. Ed.*, 2011, **50**, 12316.
132 M. Lim, D. Kim, C. Park, Y. Lee, S. Han, Z. Li, R. Williams and I. Park, *ACS Nano*, 2012, **6**, 598.
133 R. Tenne, L. Margulis, M. Genut and G. Hodes, *Nature*, 1992, **360**, 444.
134 Z. X. Wang, S. X. Zhou and L. M. Wu, *Adv. Funct. Mater.*, 2007, **17**, 1790.
135 C. H. Ye, Y. Bando, G. Z. Shen and D. Golberg, *Angew. Chem., Int. Ed.*, 2006, **45**, 4922.
136 M. S. Sander, M. J. Cote, W. Gu, B. M. Kile and C. P. Tripp, *Adv. Mater.*, 2004, **16**, 2052.
137 G. R. Patzke, F. Krumeich and R. Nesper, *Angew. Chem., Int. Ed.*, 2002, **41**, 2446.
138 M. Adachi, Y. Murata, M. Harada and S. Yoshikawa, *Chem. Lett.*, 2000, 942.
139 S. Z. Chu, S. Inoue, K. Wada, D. Li, H. Haneda and S. Awatsu, *J. Phys. Chem. B*, 2003, **107**, 6586.
140 O. K. Varghese, D. W. Gong, M. Paulose, K. G. One, E. C. Dickey and C. A. Grimes, *Adv. Mater.*, 2003, **15**, 624.
141 S. Uchida, R. Chiba, M. Tomiha, N. Masaki and M. Shirai, *Electrochemistry*, 2002, **70**, 418.
142 M. Adachi, Y. Murata, I. Okada and S. Yoshikawa, *J. Electrochem. Soc.*, 2003, **150**, G488.
143 C. Yan and D. Xue, *J. Phys. Chem. B*, 2005, **109**, 12358.
144 C. Yan, D. Xue, L. Zou, X. Yan and W. Wang, *J. Cryst. Growth*, 2005, **282**, 448.
145 C. Yan, D. Xue and L. Zou, *Mater. Res. Bull.*, 2006, **41**, 2341.
146 C. Yan, D. Xue and L. Zou, *J. Alloys Compd.*, 2008, **453**, 87.
147 G. D. Moon, S. Ko, Y. Xia and U. Jeong, *ACS Nano*, 2010, **4**, 2307.
148 A. Cabot, R. K. Smith, Y. Yin, H. Zheng, B. M. Reinhard, H. Liu and A. P. Alivisatos, *ACS Nano*, 2008, **2**, 1452.
149 X. Zhang, Z. Xu, S. Tang, Y. Deng and Y. Du, *Cryst. Growth Des.*, 2011, **11**, 2852.
150 N. H. Chou and R. E. Schaak, *Chem. Mater.*, 2008, **20**, 2081; M. Pang, J. Hu and H. C. Zeng, *J. Am. Chem. Soc.*, 2010, **132**, 10771.
151 S. Y. Jang, Y. M. Song, H. S. Kim, Y. J. Cho, Y. S. Seo, G. B. Jung, C. W. Lee, J. Park, M. Jung, J. Kim, B. Kim, J. G. Kim and Y. J. Kim, *ACS Nano*, 2010, **4**, 2391.
152 J. M. Luther, H. Zheng, B. Sadtler and A. P. Alivisatos, *J. Am. Chem. Soc.*, 2009, **131**, 16851.
153 X. Hu, Y. Masuda, T. Ohji and K. Kato, *J. Am. Ceram. Soc.*, 2010, **93**, 881.
154 H. Niu and M. Gao, *Angew. Chem., Int. Ed.*, 2006, **45**, 6462.
155 O. Kahn and C. J. Martinez, *Science*, 1998, **279**, 44.
156 K. Kuroiwa, T. Shibata, A. Takada, N. Nemoto and N. Kimizuka, *J. Am. Chem. Soc.*, 2004, **126**, 2016.
157 D. Olea, S. S. Alexandre, P. Ano-Ochoa, A. Guijarro, F. Jesffls, J. M. Soler, P. J. Pablo, F. Zamora and J. GLmez-Herrero, *Adv. Mater.*, 2000, **12**, 1761.
158 N. Kimizuka, N. Oda and T. Kunitake, *Inorg. Chem.*, 2000, **39**, 2684.
159 H. Tong, Y. Zhu, L. Yang, L. Li and L. Zhang, *Angew. Chem., Int. Ed.*, 2006, **45**, 7739.
160 E. H. Sargent, *Adv. Mater.*, 2005, **17**, 515.

161 W. G. Lu, J. Y. Fang, K. L. Stokes and J. Lin, *J. Am. Chem. Soc.*, 2004, **126**, 11798.
162 Z. Y. Zhou, Z. Z. Huang, D. J. Chen, Q. Wang, N. Tian and S. G. Sun, *Angew. Chem., Int. Ed.*, 2010, **49**, 411.
163 J. A. Zhang, M. R. Langille, M. L. Personick, K. Zhang, S. Li and C. A. Mirkin, *J. Am. Chem. Soc.*, 2010, **132**, 14012.
164 A. R. Tao, S. Habas and P. Yang, *Small*, 2008, **4**, 310.
165 T. Ming, W. Feng, Q. Tang, F. Wang, L. D. Sun, J. F. Wang and C. H. Yan, *J. Am. Chem. Soc.*, 2009, **131**, 16350.
166 T. Ming, W. Feng, Q. Tang, F. Wang, L. Sun, J. Wang and C. Yan, *J. Am. Chem. Soc.*, 2009, **131**, 16350.
167 C. L. Lu, K. S. Prasad, H. L. Wu, J. A. Ho and M. H. Huang, *J. Am. Chem. Soc.*, 2010, **132**, 14546.
168 N. Tian, Z. Zhou and S. Sun, *Chem. Commun.*, 2009, 1502.
169 N. Tian, Z. Zhou, N. Yu, L. Wang and S. Sun, *J. Am. Chem. Soc.*, 2010, **132**, 7580.
170 M. Jin, H. Zhang, Z. Xie and Y. Xia, *Angew. Chem., Int. Ed.*, 2011, **50**, 7850.
171 J. A. Zhang, M. R. Langille, M. L. Personick, K. Zhang, S. Y. Li and C. A. Mirkin, *J. Am. Chem. Soc.*, 2010, **132**, 14012.
172 J. A. Venables, *Introduction to Surface and Thin Film Processes*, Cambridge University Press, Cambridge, 2000, p. 4.
173 F. Wang, C. Li, L. Sun, H. Wu, T. Ming, J. Wang, J. Yu and C. Yan, *J. Am. Chem. Soc.*, 2011, **133**, 1106.
174 F. Wang, C. H. Li, L. D. Sun, H. S. Wu, T. Ming, J. F. Wang, J. C. Yu and C. H. Yan, *J. Am. Chem. Soc.*, 2011, **133**, 1106.
175 Y. Ma, Q. Kuang, Z. Jiang, Z. Xie, R. Huang and L. Zheng, *Angew. Chem., Int. Ed.*, 2008, **47**, 8901.
176 X. Huang, Z. Zhao, J. Fan, Y. Tan and N. Zheng, *J. Am. Chem. Soc.*, 2011, **133**, 4718.
177 D. Y. Kim, S. H. Im and O. Park, *Cryst. Growth Des.*, 2010, **10**, 3321.
178 N. Tian, Z. Zhou, N. Yu, L. Wang and S. Sun, *J. Am. Chem. Soc.*, 2010, **132**, 7580.
179 Y. Yu, Q. Zhang, B. Liu and J. Lee, *J. Am. Chem. Soc.*, 2010, **132**, 18258.
180 F. Rosei and R. Rosei, *Surf. Sci.*, 2002, **500**, 395.
181 G. A. Somorjai, *Chemistry in Two Dimensions: Surfaces*, Cornell University Press, Ithaca, 1981.
182 Q. Gong, X. Qian, P. Zhou, X. Yu, W. Du and S. Xu, *J. Phys. Chem. C*, 2007, **111**, 1935.
183 Y. D. Yin, R. M. Rioux, C. K. Erdonmez, S. Hughes, G. A. Somorjai and A. P. Alivisatos, *Science*, 2004, **304**, 711.
184 G. D. Moon, S. Ko, Y. Min, J. Zeng, Y. Xia and U. Jeong, *Nano Today*, 2011, **6**, 186.
185 U. Jeong and Y. Xia, *Angew. Chem., Int. Ed.*, 2005, **44**, 3099.
186 B. Gates, Y. Wu, Y. Yin, P. Yang and Y. Xia, *J. Am. Chem. Soc.*, 2001, **123**, 11500.
187 G. D. Moon, S. Ko, Y. Xia and U. Jeong, *ACS Nano*, 2010, **4**, 2307.
188 A. Cabot, R. K. Smith, Y. Yin, H. Zheng, B. M. Reinhard, H. Liu and A. P. Alivisatos, *ACS Nano*, 2008, **2**, 1452.
189 X. Kong, Y. Ding, R. Yang and Z. Wang, *Science*, 2004, **303**, 1348.
190 G. Z. Shen and D. Chen, *J. Am. Chem. Soc.*, 2006, **128**, 11762.
191 C. Yan and D. Xue, *J. Phys. Chem. B*, 2006, **110**, 7102.
192 H. Zeng, *J. Mater. Chem.*, 2006, **16**, 649.
193 Q. Peng, X. Sun, J. Spagnola, C. Saquing, S. Khan, R. Spontak and G. Parsons, *ACS Nano*, 2009, **3**, 546.
194 H. J. Fan, M. Knez, R. Scholz, D. Hesse, K. Nielsch, M. Zacharias and U. Gosele, *Nano Lett.*, 2007, **7**, 993.
195 M. Park, Y. Cho, K. Kim, J. Kim, M. Liu and J. Cho, *Angew. Chem., Int. Ed.*, 2011, **50**, 9647.
196 Q. Yong, Y. Yang, R. Scholz, E. Pippel, X. Lu and M. Knez, *Nano Lett.*, 2011, **11**, 2503.
197 H. Peng, C. Xie, D. T. Schoen, K. McIlwrath, X. F. Zhang and Y. Cui, *Nano Lett.*, 2007, **7**, 3734.
198 W. Oh, S. Kim, M. Choi, C. Kim, Y. Jeong, B. Cho, J. Hahn and J. Jang, *ACS Nano*, 2010, **4**, 5301.
199 X. Liang, X. Wang, Y. Zhuang, B. Xu, S. Kuang and Y. Li, *J. Am. Chem. Soc.*, 2008, **130**, 2736.
200 Y. W. Wang, H. Xu, X. B. Wang, X. Zhang, H. M. Jia, L. Z. Zhang and J. R. Qiu, *J. Phys. Chem. B*, 2006, **110**, 13835.
201 A. Colder, F. Huisken, E. Trave, G. Ledoux, O. Guillois, C. Reynaud, H. Hofmeister and E. Pippel, *Nanotechnology*, 2004, **15**, L1.
202 A. Mews, A. Eychmuller, M. Giersig, D. Schooss and H. Weller, *J. Phys. Chem.*, 1994, **98**, 934.
203 E. D. Ryu, S. W. Kim, E. J. Jang, S. N. Jun, H. S. Jang, B. K. Kim and S.-W. Kim, *Chem. Mater.*, 2009, **21**, 573.
204 R. Xie, M. Rutherford and X. Peng, *J. Am. Chem. Soc.*, 2009, **131**, 5691.
205 P. Reiss, M. Protiere and L. Li, *Small*, 2009, **5**, 154.
206 D. Battaglia, J. J. Li, Y. J. Wang and X. G. Peng, *Angew. Chem., Int. Ed.*, 2003, **42**, 5035.
207 S. Xu, J. Ziegler and T. Nann, *J. Mater. Chem.*, 2008, **18**, 2653.
208 W. K. Bae, K. Char, H. Hur and S. Lee, *Chem. Mater.*, 2008, **20**, 531.
209 X. H. Zhong, R. G. Xie, Y. Zhang, T. Basche and W. Knoll, *Chem. Mater.*, 2005, **17**, 4038.
210 L. Li, T. J. Daou, I. Texier, T. T. K. Chi, N. Q. Liem and P. Reiss, *Chem. Mater.*, 2009, **21**, 2422.
211 S. Kim, J. Park, T. Kim, E. Jang, S. Jun, H. Jang, B. Kim and S. W. Kim, *Small*, 2011, **7**, 70.
212 H. Fan, U. Goesele and M. Zacharias, *Small*, 2007, **3**, 1660.
213 R. Davies, G. A. Schurr, P. Meenan, R. D. Nelson, H. E. Bergna, C. A. S. Brevett and R. H. Goldbaum, *Adv. Mater.*, 1998, **10**, 1264.
214 F. Caruso, *Adv. Mater.*, 2001, **13**, 11.
215 S. Zhang, C. Pelligra, G. Keskar, J. Jiang, P. W. Majewski, A. D. Taylor, S. Ismail-Beigi, L. D. Pfefferle and C. O. Osuji, *Adv. Mater.*, 2012, **24**, 82.
216 J. M. Pietryga, D. J. Werder, D. J. Williams, J. L. Casson, R. D. Schaller, V. I. Klimov and J. A. Hollingsworth, *J. Am. Chem. Soc.*, 2008, **130**, 4879.
217 K. Lambert, B. D. Geyter, I. Moreels and Z. Hens, *Chem. Mater.*, 2009, **21**, 778.

218 M. Casavola, M. A. van Huis, S. Bals, K. Lambert, Z. Hens and D. Vanmaekelbergh, *Chem. Mater.*, 2012, **24**, 294.
219 H. Cheng, B. Huang, Y. Liu, Z. Wang, X. Qin, X. Zhang and Y. Dai, *Chem. Commun.*, 2012, **48**, 9729.
220 C. Yan, W. Xi, W. Si, J. Deng and O. G. Schmidt, *Adv. Mater*, 2013, **25**, 539.
221 J. Deng, H. Ji, C. Yan, J. Zhang, W. Si, S. Baunack, S. Oswald, Y. F. Mei and O. G. Schmidt, *Angew. Chem., Int. Ed.*, 2013, **52**, 2326.
222 L. Zhang, H. B. Wu and X. W. Lou, *J. Am. Chem. Soc.*, 2013, **135**, 10664.
223 W. L. Yang, L. Zhang, Y. Hu, Y. J. Zhong, H. B. Wu and X. W. Lou, *Angew. Chem., Int. Ed.*, 2012, **51**, 11501.
224 Z. Y. Wang and X. W. Lou, *Adv. Mater*, 2012, **24**, 4124.
225 Z. Y. Wang, D. Luan, C. M. Li, F. B. Su, S. Madhavi, F. Boey and X. W. Lou, *J. Am. Chem. Soc.*, 2010, **132**, 16271.
226 Y. Yao, M. T. McDowell, I. Ryu, H. Wu, N. Liu, L. Hu, W. D. Nix and Y. Cui, *Nano Lett.*, 2011, **11**, 2949.
227 H. Cheng, B. Huang, Y. Liu, Z. Wang, X. Qin, X. Zhang and Y. Dai, *Chem. Commun.*, 2012, **48**, 9729.
228 J. Lee, J. Park and H. Song, *Adv. Mater.*, 2008, **20**, 1523.
229 N. Zhang, S. Ouyang, T. Kako and J. Ye, *Chem. Commun.*, 2012, **48**, 9894.
230 H. Liu, T. Liu, X. Wu, L. Li, L. Tan, D. Chen and F. Tang, *Adv. Mater.*, 2012, **24**, 755.

